J. Fluid Mech. (1992), *vol.* 236, *pp.* 319–348
Printed in Great Britain

Experiments on mixing in continuous chaotic flows

By H. A. KUSCH[1] AND J. M. OTTINO[2]

[1] Chevron Oil Field Research Company, La Habra, CA 90633, USA

[2] Department of Chemical Engineering, Northwestern University, Evanston, IL 60208, USA

(Received 10 May 1991 and in revised form 12 August 1991)

We present the design and operation of a flow apparatus for investigations of mixing in time-periodic and spatially periodic chaotic flows. Uses are illustrated in terms of two devices operating in the Stokes regime: the *partitioned-pipe mixer*, a spatially periodic system consisting of sequences of flows in semicircular ducts, and the *eccentric helical annular mixer*, a time-periodic velocity field between eccentric cylinders with a superposed Poiseuille flow; other mixing flows can be implemented with relative ease. Fundamental differences between spatially periodic and time-periodic duct flows are readily apparent. Steady spatially periodic systems show segregated KAM-tubes coexisting with chaotic advection; such tubes are remarkably stable under a variety of experimental conditions. Time-periodic duct flows lead to complex streakline structures; since regular regions in the cross-sectional flow move through space, a streakline can find itself injected in a regular domain for some time then be trapped in a chaotic region, and so on, leading to 'intermittent' behaviour.

1. Introduction

Mixing of viscous fluids plays an important role in many industrial processes; examples include polymer processing, various types of biochemical and biomedical processes, food engineering, and materials processing. In the context of polymers the most obvious examples include blending of molten polymers to produce blends of unique properties and reactive mixing in various types of extruders utilized as continuous reactors. It is apparent that new technological developments will necessitate a deeper understanding of fluid mixing; for example new polymer applications are increasingly integrating mixing, reaction, and devolatilization into one continuous process. However, designing polymer mixing operations from first principles is still not feasible and it is therefore not surprising that current designs are based on trial and error and closely guarded empiricisms. Similar comments apply to other areas as well. The need for basic understanding of mixing was forcefully articulated by J. R. A. Pearson in the 25th anniversary issue of this journal (Pearson 1981):

I have come across relatively few practising chemical engineers who make creative use of fluid mechanics... Mixing in liquids – blending, agitation, dissolution, emulsification, or just plain stirring – is a typical issue. The process is inseparable from the mechanics of the flow employed; in many cases, the rheological properties of the fluid... are dependent on the local proportions and state of the various constituents of the mixture, i.e. on the degree and uniformity of the mixing. So there can be strong coupling between the mixing flow and the material being mixed. This is well known in a general sense to engineers, but there is little formal theory for them to refer to... Seldom is a student presented with much overall insight into the differing contributions made by different flow fields... or into the objectives

of mixing processes, which may include heat transfer and aggregation or disaggregation of a dispersed phase.

Even though we are still some way off from addressing all the points raised by these comments it is apparent, however, that the picture has improved somewhat since Pearson's dictum in 1981. New concepts based on dynamical systems and chaos (Aref 1984) have revived interest in mixing and a few aspects of the problem, especially mixing in slow flows, are beginning to be understood (for a general review see Ottino 1989; a useful collection of references is given in Aref 1991). In particular, experiments have demonstrated the applicability of these ideas and a few two-dimensional velocity fields have been studied in some detail (e.g. Chaiken *et al.* 1986; Chien, Rising & Ottino 1986; Leong & Ottino 1989; Swanson & Ottino 1990; Solomon & Gollub 1988). There is, however, a need to extend the results to more complex systems such as three-dimensional configurations, blending processes involving immiscible liquids, and systems with complex rheology. Here we consider the first of these three possibilities.

It has been known for over two decades that chaos is possible in steady three-dimensional velocity fields. This finding goes back to Hénon (1966) who showed numerical evidence of chaos in a Beltrami flow – a steady, spatially periodic solution to Euler's equation – known today as the ABC flow (Dombre *et al.* 1986). At the other end of the spectrum are the recent examples of Bajer & Moffatt (1990) and Stone, Nadim & Strogatz (1991) of chaotic Stokes flows within a spherical droplet. However, the possibility of realizing these systems in the laboratory seems remote. This leaves a few choices amenable to both experimentation and computation. Here we focus on the possibility of generating chaos in time-periodic and spatially periodic duct flows. Examples of such flows are the *partitioned pipe mixer* model (PPM) developed by Khakhar, Franjione & Ottino (1987), the *twisted pipe* model (TP) of Jones, Thomas & Aref (1989), and the *eccentric helical annular mixer* (EHAM, Ottino 1989). The PPM is a sequence of rectangular plates held stationary inside a rotating tube, whereas the TP is a sequence of half-tori each rotated by a 'pitch angle' with respect to its neighbours; both of these systems are spatially periodic. The EHAM consists of an axial Poiseuille flow between eccentric cylinders whose rotation rates are modulated periodically in time. Previous studies have addressed the behaviour of the PPM and TP flows (Khakhar *et al.* 1987; Jones *et al.* 1989); however, these models involve approximations, e.g. neglecting entrance flows, and it is important to check if experiments substantiate the computational predictions. The model for the EHAM, on the other hand is 'exact' in the sense that it does not involve any approximations beyond that of Stokes flow.

In this work we present experimental results obtained from a new apparatus capable of generating both time-periodic and spatially periodic duct flows. The case of spatially periodic flows is illustrated with the PPM whereas the case of time-periodic duct flows is illustrated with the EHAM; none of these flows appears to have been studied before. Both systems are operated under the Stokes flow regime. There is an important advantage to this mode of operation with Newtonian fluids; the axial and cross-sectional velocity fields are independent and this allows for considerable control of the mixing before the material exits the system.

The results presented are primarily experimental but supporting computations are provided as well. However, as opposed to previous studies involving two-dimensional velocity fields, the experimental assessment of chaos is mostly qualitative, that is, we do not identify horseshoe maps as done previously by Chien *et al.* (1986). This,

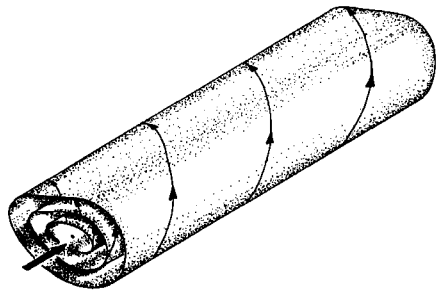

FIGURE 1. Conceptual sketch of a duct flow.

however, should pose no serious difficulties as the demarcation between regular and chaotic behaviour will be readily apparent. The organization of the paper is as follows: §2 gives some foundation regarding regular duct flows as well as a brief introduction to both the PPM and EHAM. Section 3 describes the experimental apparatus, computer control, and flow visualization conditions. Section 4 is divided into two parts and is devoted to the presentation and interpretation of key experimental results. Finally, §5 is devoted to possible extensions of the experimental results.

2. Mixing in continuous flows

2.1. *Regular duct flows*

Regular duct flows are composed of a bounded two-dimensional cross-sectional velocity field with stream function $\psi(x_1, x_2)$ augmented by a steady unidirectional axial flow

$$\frac{\mathrm{d}x_1}{\mathrm{d}t} = u_1 = \frac{\partial \psi}{\partial x_2}, \tag{1}$$

$$\frac{\mathrm{d}x_2}{\mathrm{d}t} = u_2 = -\frac{\partial \psi}{\partial x_1}, \tag{2}$$

$$\frac{\mathrm{d}x_3}{\mathrm{d}t} = u_3 = v(x_1, x_2), \tag{3}$$

where

$$\frac{\partial \psi}{\partial t} = \frac{\partial \psi}{\partial x_3} = \frac{\partial v}{\partial t} = \frac{\partial v}{\partial x_3} = 0. \tag{4}$$

A typical picture is shown in figure 1; the combination of the cross-sectional flow with the unidirectional axial flow causes a particle to follow a helical path. The stretching of infinitesimal material vectors in such flows can be calculated as follows (Franjione & Ottino 1991). After a given time T, a particle returns to its initial position in the cross-sectional projection while at the same time it moves down the duct axis. A fluid particle initially located at $\boldsymbol{X} = (X_1, X_2, X_3)$ at time t finds itself at $(X_1, X_2, X_3 + f(X_1, X_2))$ at time $t+T$, where f is given by

$$f = \int_0^T v(\phi(\boldsymbol{X}, t'))\,\mathrm{d}t' \tag{5}$$

and $\phi(\boldsymbol{X}, t)$ is the cross-sectional motion (the period of recirculation T depends on which stream surface the particle is located on). However, a particle which initially

is located very near $\boldsymbol{X}$ (i.e. at $\boldsymbol{X}+\mathrm{d}\boldsymbol{X}$) does not return to the same position in the cross-sectional after a time T. The vector $\mathrm{d}\boldsymbol{X}$ attached to the particle $\boldsymbol{X}$ evolves as

$$\mathrm{d}\boldsymbol{x}_{nT} = (\boldsymbol{1}-\boldsymbol{M})^n \cdot \mathrm{d}\boldsymbol{X} \tag{6}$$

where

$$\boldsymbol{M} = \begin{bmatrix} u_1 \dfrac{\partial T}{\partial X_1} & u_1 \dfrac{\partial T}{\partial X_2} & 0 \\ u_2 \dfrac{\partial T}{\partial X_1} & u_2 \dfrac{\partial T}{\partial X_2} & 0 \\ -\dfrac{\partial f}{\partial X_1} & -\dfrac{\partial f}{\partial X_2} & 0 \end{bmatrix} \tag{7}$$

and $\mathrm{d}\boldsymbol{x}_{nT}$ is the state of $\mathrm{d}\boldsymbol{X}$ after n periods of length T. Since $\boldsymbol{M}^2$ is identically zero, it can be shown that as long as the elements of $\boldsymbol{M}$ are bounded, the length of $\mathrm{d}\boldsymbol{x}$ increases as t, indicating that mixing is poor. (Note that this result is more general than that corresponding to steady curvilinear flows (Noll 1962; Ottino 1989). $\boldsymbol{M}^2$ is identically zero since both $\boldsymbol{v}\cdot\boldsymbol{\nabla}_{\boldsymbol{X}}T$ and $\boldsymbol{v}\cdot\boldsymbol{\nabla}_{\boldsymbol{X}}f$ are zero ($\boldsymbol{\nabla}_{\boldsymbol{X}}$ is the gradient with respect to X_1, X_2).)

Regular duct flows can be made chaotic by exploiting analogies with two-dimensional flows. The first possibility is to make the cross-sectional flow time-periodic; the second possibility is to make the cross-sectional flow spatially periodic. A necessary, but not sufficient condition, is that the streamline portraits at two successive times or axial distances show crossing of streamlines. In this case the length stretch in chaotic regions is exponential.

2.2. *The PPM flow*

The partitioned pipe mixer (PPM) consists of a pipe of radius R partitioned into a sequence of semicircular ducts by rectangular plates of length L placed orthogonally to each other; the system can be regarded as an idealized version of a commercial mixer called the Kenics static mixer (Middleman 1977). A sketch of the PPM model and the cross-sectional streamlines of the model flow are shown in figure 2(*a*). The axial flow is driven by a pressure gradient. The solution for a semicircular duct of radius R is

$$v_z = \langle v_z \rangle \sum_{k=1}^{\infty} \left\{ \left(\frac{r}{R}\right)^{2k-1} - \left(\frac{r}{R}\right)^2 \right\} \frac{\sin\left[(2k-1)\theta\right]}{(2k-1)\{4-(2k-1)^2\}}, \tag{8}$$

where the average velocity is given by

$$\langle v_z \rangle = \frac{8-\pi^2}{4\pi\mu} \frac{\partial P}{\partial z} R^2. \tag{9}$$

The two-dimensional cross-sectional flow satisfies

$$\nabla^4 \psi = 0, \tag{10}$$

with boundary conditions

$$\psi = \frac{1}{r}\frac{\partial \psi}{\partial \theta} = 0; \quad -\frac{\partial \psi}{\partial r} = v_R \quad \text{for} \quad r = R \quad \text{and} \quad \theta \in [0, \pi) \tag{11a}$$

$$\psi = \frac{1}{r}\frac{\partial \psi}{\partial \theta} = \frac{\partial \psi}{\partial r} = 0 \quad \text{for} \quad \theta = 0, \pi \quad \text{and} \quad r \in [0, R). \tag{11b}$$

A one-term weighted-residuals solution of (10), (11) is

$$\psi = \frac{4 v_R R}{3\gamma} \left(\frac{r}{R}\right)^2 \left\{ 1 - \left(\frac{r}{R}\right)^{\gamma} \right\} \sin^2 \theta, \tag{12}$$

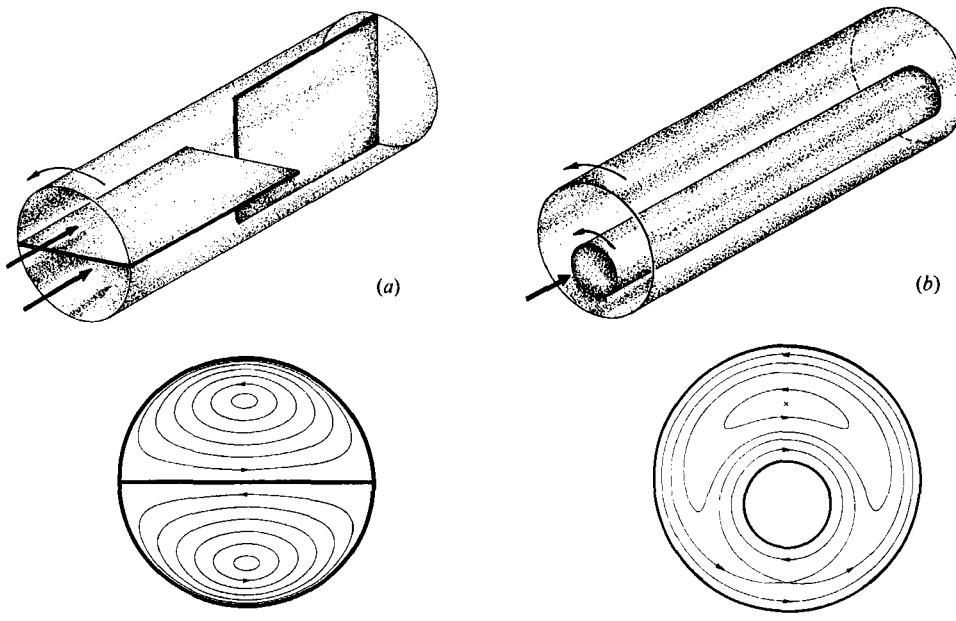

FIGURE 2. Conceptual sketches of two continuous chaotic mixers and representative cross-sectional streamlines: (*a*) PPM; (*b*) EHAM.

with $\gamma = (11/3)^{\frac{1}{2}} - 1$ (Khakhar 1986). The velocity field, with the v_z-component described by a three-term approximation, is given by

$$v_r = \frac{\mathrm{d}r}{\mathrm{d}t} = \beta r(1 - r^\gamma)\sin 2\theta, \tag{13a}$$

$$\frac{v_\theta}{r} = \frac{\mathrm{d}\theta}{\mathrm{d}t} = -\beta\{2 - (2+\gamma)r^\gamma\}\sin^2\theta, \tag{13b}$$

$$v_z = \frac{\mathrm{d}z}{\mathrm{d}t} = \frac{16}{\pi^2 - 8}\sum_{k=1}^{3}\{r^{2k-1} - r^2\}\frac{\sin[(2k-1)\theta]}{(2k-1)\{4-(2k-1)^2\}} \tag{13c}$$

(the velocities are made dimensionless by normalizing axial distances by L, radial distances by R, and time by $L/\langle v_z\rangle$). The behaviour of the system is thus described by a single parameter, β, the *mixing strength*, defined as

$$\beta = \frac{4v_R L}{3\gamma\langle v_z\rangle R} \tag{14}$$

(β can be considered as the product of the characteristic residence time, $L/\langle v_z\rangle$, and the cross-sectional shear rate, v_R/R). The physical picture is as follows: a fluid particle travels a helical path in each mixer element; between elements it jumps from stream surface to stream surface and a succession of two elements constitutes a unit of the flow. The basic structure of the mixing patterns can be investigated by means of Poincaré sections; they can be generated by recording intersections of selected trajectories with the surfaces of sections placed at distances $2L$ apart in a very long – ideally, infinitely long – mixer, and then projecting all the intersections onto a plane parallel to the surfaces. Such computations indicate that the details of the axial velocity field have a major effect on the structure of Poincaré sections, and thus on the cross-sectional mixing and dispersion. For example, Poincaré sections corre-

sponding to plug axial flow (perfect slip at the wall) are quite different from those corresponding to Poiseuille flow. The most important result, however, is that all systems display a similar structure independent of the details of the axial flows: regular KAM-tubes prevent effective cross-sectional mixing and particles inside the KAM-tubes cannot mix with the rest of the flow (Ottino 1989).

It is rather clear that this model is only an approximation. Note for example that the velocity can be written as

$$\boldsymbol{v}_{\mathrm{PPM}} = (1-H(z-1))\,\boldsymbol{v}(\theta)+H(z-1)\,\boldsymbol{v}(\theta+\tfrac{1}{2}\pi), \tag{15}$$

where $\boldsymbol{v}(\theta) = (v_r, v_\theta, v_z)$ (see (13*a–c*)) is a function of (r, θ), and $\boldsymbol{v}(\theta+\frac{1}{2}\pi)$ is the velocity field after it has been rotated by 90° ($H(z-1)$ is the Heaviside step function which is 0 for $z<1$ and 1 for $z>1$). The divergence of the PPM velocity field is therefore

$$\nabla\cdot\boldsymbol{v}_{\mathrm{PPM}} = (1-H(z-1))\left\{\frac{1}{r}\left[\frac{\partial(rv_r(\theta))}{\partial r}+\frac{\partial v_\theta(\theta)}{\partial\theta}\right]\right\}$$
$$+H(z-1)\left\{\frac{1}{r}\left[\frac{\partial(rv_r(\theta+\frac{1}{2}\pi))}{\partial r}+\frac{\partial v_\theta(\theta+\frac{1}{2}\pi)}{\partial\theta}\right]\right\}-\delta(z-1)\,v_z(\theta)+\delta(z-1)\,v_z(\theta+\tfrac{1}{2}\pi), \tag{16}$$

where $\delta(z-1)$ is the Dirac delta function, which is zero everywhere except at $z=1$. The first two terms are zero by construction of the cross-sectional flow. The third and fourth terms are zero everywhere except at $z=1$ at which point $v_z(\theta) = v_z(\theta+\frac{1}{2}\pi)$ for the velocity field to be divergence free. In general, however, $v_z(\theta) \neq v_z(\theta+\frac{1}{2}\pi)$, so conservation of mass is locally violated by the PPM model. Similar comments apply to the twisted pipe model of Jones *et al.* (1989). The average of the divergence over the cross-section is zero which simply means that the total flow rate is the same before and after the junction. The key question, however, is whether or not the existence of KAM-tubes predicted by such models can actually be detected by experimental means. This is especially important in the light of the sensitivity of the computational results to the details of the axial velocity field.

2.3. *The EHAM flow*

By contrast to the PPM, the EHAM model involves no approximations beyond those of Stokes flow. The system corresponds to the flow between eccentric cylinders with a superposed pressure-driven Poiseuille flow. A sketch of the EHAM and cross-sectional streamlines for counter-rotating cylinders are shown in figure 2(*b*). In this case the system is time periodic rather than spatially periodic, there is no discontinuous jumping of particles between stream surfaces in space. An exact solution for the cross-sectional flow was found by Wannier (1950); an extensive experimental study of this system under time-periodic operation is reported by Swanson & Ottino (1990). The velocity field in the EHAM is simply a Poiseuille flow between eccentric cylinders and the solution used here is that of Snyder & Goldstein (1965). For simplicity the experiments and computations are restricted to a radius ratio (R_1/R_2) equal to 1/3, and to an eccentricity $\epsilon = e/(R_2-R_1)$, where e is the distance between centres of the cylinders, equal to 0.3.

3. Experimental

3.1. *Apparatus and design considerations*

Since the primary tool of experimental mixing studies is flow visualization, the primary design consideration is that views of the flow field must be free from obstruction. Similarities between the flows allows a common frame and outer

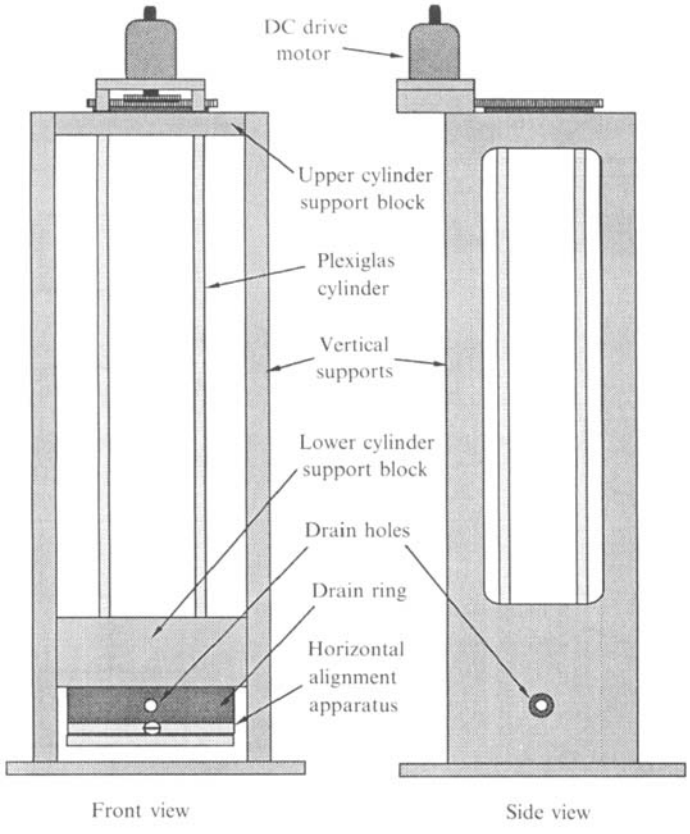

(Drawing not to scale)

FIGURE 3. Continuous chaotic mixer frame.

cylinder to serve as a basis for both mixers, and inserts are used to switch between the EHAM and PPM flows. Front and side sketches of the mixer frame and outer cylinder are shown in figure 3. The mixers are supported by a frame made of cast aluminium tooling plate. The outer cylinder is suspended from the top by the upper cylinder support block and stabilized on the bottom by the lower cylinder support block. Bronze rings are pressed into holes cut into the centres of the upper and lower cylinder support blocks; a bearing is formed between the bronze and the stainless steel tubes at the top and bottom of the outer cylinder assembly. The outer cylinder assembly consists of an 8.8 cm i.d., 10.1 cm o.d., 106 cm long Plexiglas tube separating two short, thick stainless steel tubes. The outer cylinder is rotated by a large gear mounted on the upper stainless steel tube. The open top of the outer cylinder allows considerable flexibility for addition of the working fluid and dyes. A drive motor for the outer cylinder is mounted on the upper cylinder support block. The upper and lower cylinder support blocks are held apart by two vertical supports; rounded rectangular holes in the sides of the support blocks allow side views of the flow field. The vertical supports are attached to a large aluminium base plate. Plexiglas sheets are mounted outside the vertical supports; the space between the outer cylinder and the Plexiglas sheets is filled with glycerin to reduce optical distortion from the curvature of the outer cylinder.

An aluminium drain ring is bolted to the bottom of the lower cylinder support block. Four holes (3/4 in NPT) drilled through the sides of the drain ring allow the

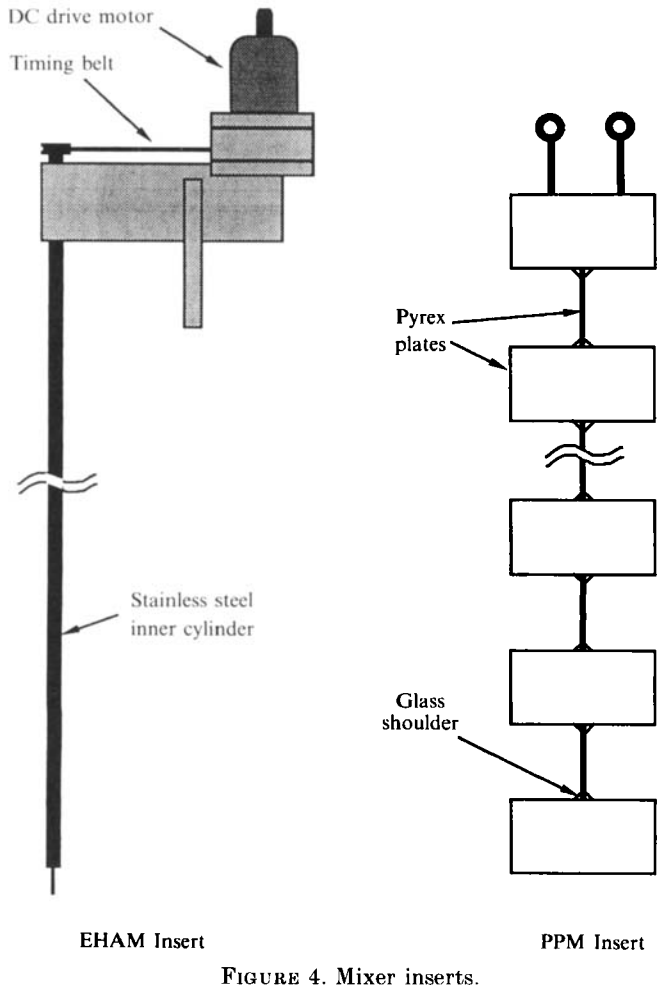

FIGURE 4. Mixer inserts.

working fluid to exit the bottom of the mixer. The horizontal alignment assembly is attached to the bottom of the drain ring. The horizontal alignment assembly is made from a 20 cm square, 1.27 cm thick, Plexiglas plate and four stainless steel machine screws. A regular octagon, 11 cm across, cut from the centre of the plate serves as the horizontal alignment plate. The horizontal alignment plate is adjusted by stainless steel screws threaded through four tapped holes in the sides of the fixed plate. Another 20 cm square Plexiglas plate is mounted below the horizontal alignment plate. The advantage of this configuration is that it allows an unobstructed view of the flow field from below, while at the same time stabilizing the mixer insert.

The only difference between the EHAM and PPM configurations are the mixer inserts. For the EHAM we add an inner cylinder assembly, while for the PPM we add a series of stationary baffles; see figure 4. The EHAM inner cylinder is a 2.93 cm diameter stainless steel rod 135 cm long. A 0.64 cm diameter stainless steel pin, 8 cm long is pressed into a hole 2 cm deep in the bottom of the inner cylinder. The top of the inner cylinder, which is only 1.27 cm diameter, passes through one end of a cantilevered arm; inside the cantilevered arm are a pair of bearings which allow the inner cylinder to turn freely. At the opposite end of the cantilevered arm is the drive

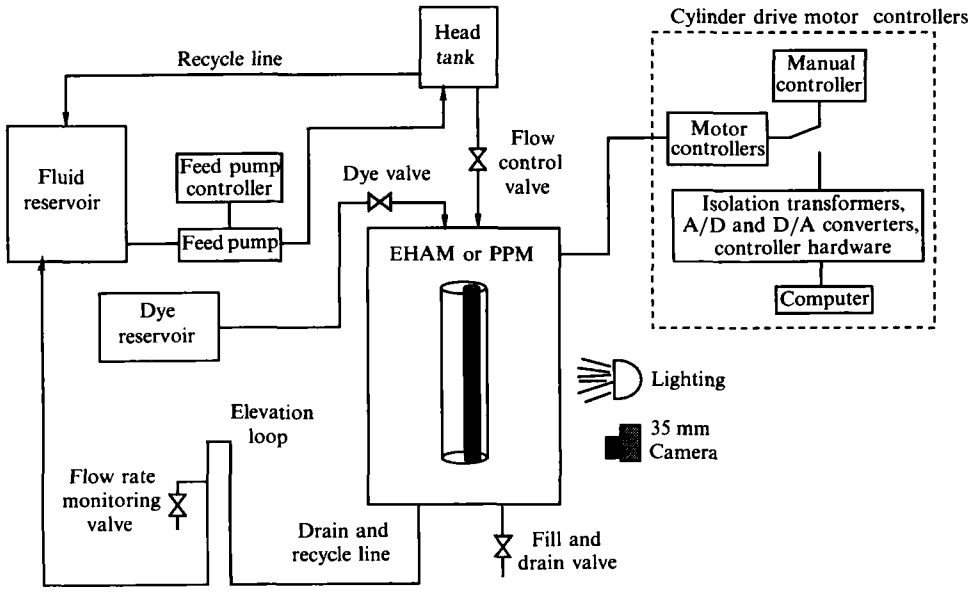

FIGURE 5. Mixer support equipment.

motor. A timing belt runs from a gear at the top of the inner cylinder to the drive motor. The inner cylinder assembly is attached to the upper cylinder support block. The entire inner cylinder apparatus is adjustable horizontally so that the eccentricity may be varied. The pin in the bottom of the inner cylinder enters a hole in the horizontal alignment plate.

One of the assumptions in the PPM model is that the plates of the mixer are infinitely thin and that they extend all the way to the cylinder wall. Obviously this is impossible to realize experimentally. As a compromise the experimental mixer insert is made of thin Pyrex plates (0.32 cm × 5.08 cm × 8.26 cm). Thinner plates and a smaller gap may be possible with metal plates, however lighting would be difficult and views of the flow field would be obstructed. Two 0.6 cm diameter glass rods, with circular loops on one end, are attached to the top plate of the PPM insert. The loops are used to suspend the insert from an aluminium frame attached to the upper cylinder support block. At the bottom, the insert rests in a 1.3 cm deep channel in a 2.5 cm × 5 cm × 20 cm Plexiglas block which is in turn attached to the horizontal alignment plate.

Another issue is developing flows. The model analysis assumes that the velocity field in each semicircular duct is fully developed, i.e. $v_z(r,\theta)$ but not $v_z(r,\theta,z)$. Experimentally, the effect of the entrance and exit flows could be minimized by making the length of the mixer segments long in comparison to the cylinder radius. Within the constraints of our frame and outer cylinder assembly, and the desire to have a reasonable number of mixer segments in the system, the length of the plates is chosen to be 5.08 cm; this gives nine mixer segments in the apparatus. Since the length of the plate is less than the cylinder radius, we expect developing flows to be important.

Peripheral to the mixer are motors, control systems, pumps, pipes and storage tanks. The entire experimental set-up is shown schematically in figure 5. The working fluid is transferred from the 30 gallon reservoir to a 5 gallon head tank by a gear pump (ECO G6, driven by a $\frac{3}{4}$ hp 90 V DC motor). The pressure in the head

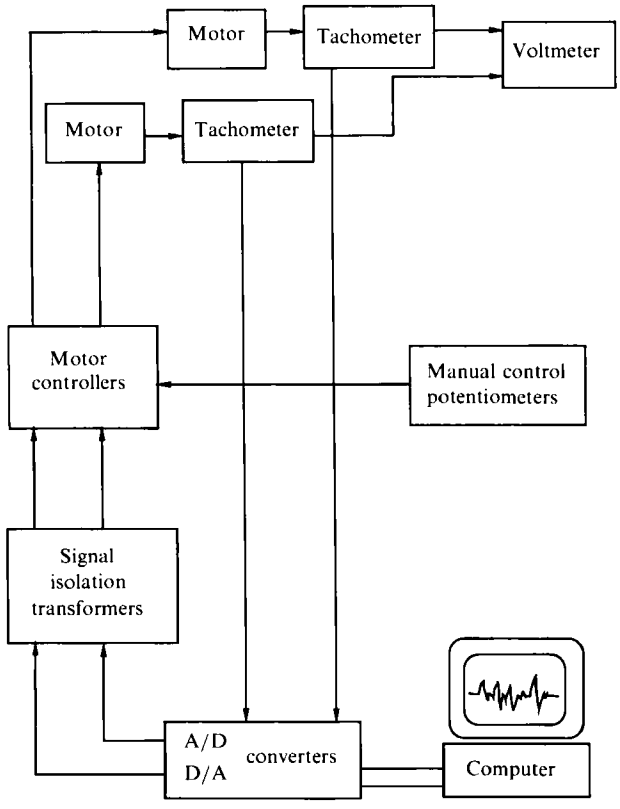

FIGURE 6. Drive-motor control hardware.

tank, mounted 1 m above the mixer, is kept constant by running the feed pump at a flow rate higher than the flow rate to the mixer: an overflow line recycles fluid back to the reservoir. The flow rate to the mixer is adjusted by a needle valve on the feed line and a strainer breaks up the entering stream. The fluid level in the mixer is kept constant by an overflow loop in the mixer drain line. The working fluid can be either recycled or discarded. Recycling the fluid is done before an experiment to homogenize concentration and thermal gradients between the mixer, head tank and the reservoir. Several other valves are used to measure the flow rate, and to fill, drain and clean the mixer.

The dye is fed directly to the mixer from elevated reservoirs and $\frac{1}{8}$ in. Nalgene polyethylene needle valves regulate the dye flow rate. The dye is injected through 20 cm long, 0.32 cm o.d., 0.16 cm i.d. stainless steel tubes and is fed 20 cm below the glycerin feed point in EHAM, or after the first mixer segment, which is 30 cm below the glycerin feed point, in the case of the PPM.

The drive motors for both cylinders are variable-speed $\frac{1}{50}$ h.p. DC motors (Bodine NSH-11D5 with 1750:1 speed reduction). The motors have been modified with 2.6 V/1000 r.p.m. tachometers (Servo-Tek SB-7427A-7) connected directly to the armatures of the motors. The control system, shown in figure 6, monitors the cylinder rotation rates and corrects for drift due to noisy line voltage in the laboratory. A PC's Limited 286 personal computer and Keithley System 570 Data Acquisition Workstation are the major hardware components of the control system. The computer runs Microsoft Quickbasic programs which call Keithley Quick500 subroutines. The subroutines create, load and access tables of digital voltages for

output to the motor control boosters or input from the tachometers. The digital tables of voltages are sent and received from the 16 bit A/D and D/A converters in the System 570. The angular displacement of the cylinders is calculated by numerically integrating the tachometer voltages which are proportional to the cylinder rotation rates. A simple proportional control scheme corrects the output voltages. The other components of the control system are the motor control boosters, which boost the 0–5 V signals from the computer and send them to the motors, and the signal isolation transformers (PentaPower KBSI-240D) which protect the computer and data acquisition hardware from spurious high-voltage spikes generated by the motor control boosters.

A Nikon FE2 camera and a Nikkor micro f/4.0 105 mm lens are used to expose 100 and 400 ASA Kodak Ektachrome colour slide film. Yellow and orange filters (Quantenary Y2 and 85A) improve resolution and reduce reflections. The fluorescent dyes (rhodamine and fluorescein, Cole Parmer L-00295-15 and L-00295-17) are stimulated by long-wavelength UV light. Two UV lamps (Spectronics XX-40) are mounted on the mixer base plate; lighting is perpendicular to the viewing direction.

3.2. *Experimental procedures*

The working fluid is glycerin (Emery 916 Glycerin 99.7% pure) diluted with water (6 glycerin:1 water) and a small amount of chlorine bleach (1 bleach:900 glycerin–water) to make the glycerin more transparent. Diluting the glycerin drops the viscosity from $O(10\ \mathrm{P})$ to $O(1\ \mathrm{P})$. This has two effects: first the gear pump can run longer without overheating; and, second, tiny air bubbles, suspended in the glycerin during transfer from the 55 gallon drums to the fluid reservoir, will float to the surface in a reasonable time.

To prepare for an experiment, glycerin is pumped from 55 gallon drums, diluted, mixed and pumped into the reservoir. Air bubbles float to the surface after the fluid has sat for one day. The fluorescent dyes are prepared by crushing the dye tablets in a mortar and pestal and then mixing the powder into undiluted glycerin. The mixture is stirred daily until the glycerin is saturated with dye; this usually takes about one week. On the day of an experiment the system is run in recycle mode, while stirring the glycerin reservoir, for about 2 h; this is typically enough time to homogenize the glycerin–water mixture in the system. The flow visualization results are extremely sensitive to slight density differences between the dye and glycerin and small density differences, of less than 1%, cause the dye to rise or sink at a noticeable rate ($O(0.5\ \mathrm{cm/min})$). As prepared, the fluorescent dyes are denser than the working fluid, therefore water is added to the dye until the densities are matched. A sample of the working fluid is taken from the flow-rate measuring valve and small samples of the diluted dye are injected with disposable pipets into the glycerin–water mixture. The densities are considered matched when a 1 cm diameter sphere of dye does not move appreciably in 10 min.

An experiment is started by setting the axial and cross-sectional velocities, allowing the control system to come to steady state, and then starting the dye streak. Photographs are taken after the streaklines have fully developed. In the PPM this occurs when there is no new dye interface formed in the flow. In the EHAM the flow is changing continuously and the assessment is a bit more problematic; in this case we study the small-scale structures produced at the exit of the mixer and determine when they do not change between periods. In both flows the time to reach steady state is determined primarily by the axial flow rate, but a typical time is about 30 min. The dye is turned off after the pictures have been taken and the dye

remaining in the mixer is allowed to drain. When the working fluid in the mixer is dye free, the procedure is repeated. A single experimental run takes between 6 and 10 h and four to six experiments can be performed with the 30 gallons of fluid in the glycerin reservoir. Owing to the high cost of glycerin, an exhaustive search of the parameter space is rather impractical; we estimate that the experiments reported here consumed 750 gallons of glycerin.

3.3. *Experimental uncertainties*

Before discussing experimental results a discussion of experimental uncertainties is in order. The largest sources of uncertainty are the axial and cross-sectional velocities. In the laboratory, the velocities are not measured directly but instead they are inferred from other information. The cylinder angular velocities are measured by monitoring the output of tachometers attached directly to the armatures of the cylinder drive motors. There is a linear relationship between the angular velocity of the cylinder and the tachometer voltage. The tachometer voltage shows high-frequency noise about the mean voltage and low-frequency drift of the mean voltage. The low-frequency drift is corrected by the control system, but the random noise, with maximum amplitude of ± 0.02 V, independent of the mean voltage, is uncontrolled; the measurement uncertainty is ± 0.005 V. The axial velocity is obtained from the flow rate, which is measured with a 500 ml graduated cylinder and a stop watch; the uncertainty in this measurement is ± 5 ml/min. Although there is no feedback control on the axial velocity, the axial flow rate is constant for hours.

The velocity uncertainties can be quantified in terms of the Reynolds numbers. The axial and cross-sectional Reynolds numbers for the EHAM are

$$Re_{\text{EHAM:axial}} = \frac{\rho \langle v_z \rangle (R_2 - R_1)}{\mu}, \tag{17}$$

$$Re_{\text{EHAM:cs}} = \frac{\rho V (R_2 - R_1)}{\mu}, \tag{18}$$

where ρ is the density, μ the viscosity, R_2 the outer cylinder radius, R_1 the inner cylinder radius, $\langle v_z \rangle$ the average axial velocity and V a characteristic cross-sectional velocity, which we take as $|v_1|_{\max} + |v_2|_{\max}$. The axial and cross-sectional Reynolds numbers for the PPM are

$$Re_{\text{PPM:axial}} = \frac{\rho \langle v_z \rangle R}{\mu}, \tag{19}$$

$$Re_{\text{PPM:cs}} = \frac{\rho v_R R}{\mu}, \tag{20}$$

where R is the cylinder radius, and v_R the cylinder velocity. For the experiments reported here the viscosity, density, inner cylinder radius and outer cylinder radius are 1.1 P, 1.2 g/cm^3, 1.47 cm and 4.4 cm, respectively. The Reynolds numbers, in terms of the measured quantities, are

$$Re_{\text{EHAM:axial}} = 9.9 \times 10^{-4} Q \text{ min cm}^{-3} \pm 0.005, \tag{21}$$

$$Re_{\text{EHAM:cs}} = 0.96 E_1 \text{ V}^{-1} + 0.93 E_2 \text{ V}^{-1} \pm 0.03, \tag{22}$$

$$Re_{\text{PPM:axial}} = 1.3 \times 10^{-3} Q \text{ min cm}^{-3} \pm 0.007 \tag{23}$$

$$Re_{\text{PPM:cs}} = 1.4 E_2 \text{ V}^{-1} \pm 0.03. \tag{24}$$

where Q is the axial flow rate, E_1 is the magnitude of the tachometer voltage from the inner cylinder and E_2 is magnitude of the tachometer voltage from the outer cylinder. The ranges of operating conditions are approximately $0 \leqslant E_{1,2} \leqslant 6$ V, $0 \leqslant Q \leqslant 600$ ml/min. This gives Reynolds numbers ranges of

$$0 < Re_{\text{EHAM:axial}} < 0.6, \tag{25}$$

$$0 < Re_{\text{EHAM:cs}} < 11, \tag{26}$$

$$0 < Re_{\text{PPM:axial}} < 0.8, \tag{27}$$

$$0 < Re_{\text{PPM:cs}} < 8. \tag{28}$$

Since the absolute uncertainties in the cylinder velocities are fixed, the relative uncertainties can be minimized by maximizing the voltages and flow rate. There are trade-offs between minimizing the relative errors and satisfying creeping flow conditions. To satisfy Stokes flow conditions the voltages and flow rates must be kept to a minimum. Another problem is dye buoyancy; since it is impossible to match the densities exactly, given enough time the dye will move relative to the neighbouring fluid (in the experiments this shows up as dye streaks having rough edges). To minimize this effect the residence time in the mixer should be relatively short. The minimum axial flow rate in practice is about 200 ml/min, which gives a mean residence time of about 30 min, and axial Reynolds numbers of about 0.2 for the EHAM and 0.3 for the PPM. Diffusion of the dye is relatively unimportant at this residence time; the diffusional distance $(Dt)^{\frac{1}{2}}$ is about 0.01 cm for a diffusion coefficient $D = O(10^{-6}\ \text{cm}^2/\text{s})$ and a residence time of 30 min.

The axial and cross-sectional flow experimental uncertainties in the PPM can also be expressed in terms of the mixing strength parameter:

$$\beta = 1794\ \text{cm}^3\ \text{min}^{-1}\ \text{V}^{-1} \frac{E_2}{Q}\left\{1 \pm \left[\left(\frac{0.02}{E_2}\right)^2 + \left(\frac{5}{Q}\right)^2\right]^{\frac{1}{2}}\right\}. \tag{29}$$

For a flow rate of 200 ml/min and a tachometer voltage of about 1, the mixing strength parameter is 9 ± 0.3, the axial Reynolds number is 0.26 and the cross-sectional Reynolds number is about 1.4. At this Reynolds number, there might be questions as to whether or not the mixing is actually independent of the Reynolds number (the only way to reduce the Reynolds numbers, given the constraints and noise, is to increase the viscosity, which as discussed above, is impossible with the pump and bubbles in the system). The validity of the Stokes flow approximation in the PPM is addressed in §4.1.4.

Let us now consider the effects of time periodicity in the EHAM. If the time of diffusion of momentum is much less than the period of the cross-sectional flow perturbation ($L^2/\nu \ll T$) then the fluid responds quasi-statically to the motion of the boundaries. Equivalently,

$$\frac{L^2}{\nu T} = \frac{VL}{\nu}\frac{L}{VT} = ReSr \ll 1. \tag{30}$$

We define the Strouhal number for the EHAM as

$$Sr_{\text{EHAM}} = \frac{R_2 - R_1}{VT}. \tag{31}$$

If the product of the cross-sectional velocity and the period is small, the Strouhal number may be large. On the other hand, if the product is large, the Strouhal number will be small, as desired. The cross-sectional velocity and the period are not independent. They are related because the angular displacement of the cylinders during a period, which determines the structure of the cross-sectional chaos, is the integral of the angular velocity over a period. There is thus a trade-off in choosing the period. If the period is long, there will not be a significant number of periods of the cross-sectional flow during the fluids residence time in the mixer (i.e. there will be little cross-sectional mixing relative to the axial flow). Alternatively, if the periods are short, the Reynolds number of the cross-sectional flow will be large. Typical periods of the cross-sectional flow are between 20 and 120 s. The Strouhal number, in terms of the measured quantities, is

$$Sr_{\mathrm{EHAM}} = \frac{2.93\ \mathrm{s\ V}}{T(0.30E_1 + 0.29E_2)}\left\{1 \pm \frac{0.008\ \mathrm{V}}{0.30\mathrm{E}_1 + 0.29\mathrm{E}_2}\right\}. \tag{32}$$

At the operating conditions chosen, the Strouhal number and its uncertainty are small. The uncontrolled high-frequency noise in the tachometer output voltages results in angular displacement fluctuations of about $\pm 2°$ per period. Additional information about the experimental apparatus and procedures are available in Kusch (1991).

4. Results and interpretation

4.1. *An example of a spatially periodic system: the PPM flow*

In this section we present a few key results for the PPM flow. This system is an example of a steady, spatially periodic chaotic flow; the main parameter governing the behaviour of the system is the mixing strength β.

4.1.1. *Mixing mechanisms and existence of KAM-tubes*

Let us start by considering the primary mixing mechanisms operating in the PPM flow; these mechanisms are present in the approximate model as well. Figure 7(*a*) (plate 1) shows the evolution of two dye streaks injected into the system operating at $\beta = 10$. Immediately after leaving the injection nozzle the green dye streak is slightly stretched and then cut by a plate. Subsequently, the left side of the cut dye streak is slowly stretched in the next three mixer elements and cut again. Similarly the right side of the cut dye streak is quickly stretched in the next half-segment and is cut by the next plate. The experiment also shows evidence of a secondary flow (not accounted for by the model); the left side of the cut green dye streak moves backwards as it goes over the top edge of the second plate. It is evident that cutting is a contributing mechanism to the mixing; however, it is equally clear that chaos can occur without any cutting mechanism (as in the EHAM). In fact, it appears that the key element for generating chaos in this, as well as other flows, is the continuous shifting or modulation of streamlines. Let us consider now the global dye structures generated in the PPM flow.

Consider two experiments at $\beta = 10$; the only difference between the experiments is the location of the orange dye streak. Two distinct types of behaviour are readily apparent. In figure 7(*b*) (plate 1) both dye streaks are well mixed while in figure 7(*c*) (plate 1) the orange dye streak travels through the mixer without contacting the

yellow dye. After two mixer segments the orange dye streak returns to the same cross-sectional position; this is evidence of a KAM-tube surrounding a period-2 elliptic point. Moreover the dye streak in the KAM-tube shows very little stretching. On the opposite side of the mixer from the KAM-tube with the orange dye streak in it is another KAM-tube, identical to the one shown in the experiment, except moved down one mixer segment; the tubes spiral around each other as they move down the mixer. The spatial extent of the KAM-tubes can be seen as the dye-free oval region surrounding the dye streak. The location of the green dye streak in both experiments is the same. The flow rate and velocity are nearly identical; however, the resulting dye streaks are slightly different. This difference is primarily due to fluctuations in the thickness of the green dye streak. The patterns, however, are remarkably similar considering that the pictures were taken over two hours apart. This gives an indication of the stability and reproducibility of the experiments.

4.1.2. *Mixing behaviour as a function of the mixing strength*

Let us now consider the changes in the mixing behaviour as β is increased from zero. Figures 8(*a*) and 8(*b*) (plate 2) show experiments for $\beta = 0$ and 4. For the case of $\beta = 0$ there is no cylinder rotation and the dye streaks travel through the mixer nearly undisturbed; the flow is non-chaotic. The small waviness in the dye stream is due to the finite thickness of the plates as well as entrance and exit effects. The case corresponding to $\beta = 4$ shows that the addition of a small amount of twist greatly enhances the mixing. Computations suggest that at low values of β there should be large regions of regularity; however, in several experiments performed on this flow, no evidence of KAM-tubes was found. Note, however, that one way KAM-tubes were found experimentally, other than by trial and error, was to visually examine the flow near the exit of the mixer for regions the dye did not penetrate. This technique did not work at low mixing strengths because the mixing was not intense enough to reveal these light spots. With more mixer segments, KAM-tubes could probably be found.

Let us consider the behaviour of the KAM-tubes as β is increased. As discussed previously, and as shown in figure 8(*c*) (plate 2), there are two period-2 KAM-tubes at $\beta = 10$ and as shown in figure 8(*d–f*) (plates 2 and 3), these tubes are also present in flows at $\beta = 15$, 20, and 25. The cross-sectional area of the KAM-tubes decreases and they move towards the centre of the mixer as β is increased. We found no evidence of additional KAM-tubes; a possible reason is that new periodic elliptic points are of high period (4 or higher) and that the cross-section – as suggested by computations – is likely to be small. As the mixing strength increased further to $\beta = 30$, shown in figure 8(*g*) (plate 3), no dye initial positions can be found that are entirely within KAM-tubes. The green dye streak, however, remains partially coherent at the mixer exit. Finally, at $\beta = 40$, there is no evidence of regularity; see figure 8(*h*) (plate 3). At higher values of the mixing strength the dye injection apparatus interferes with the resulting dye streak and no reliable experiments are possible.

In spite of simplifications, the PPM model correctly predicts the coexistence of chaos and regularity. However, the experiments show that the shape of the KAM-tubes are remarkably independent of the mixing strength whereas computations show considerably more variability. Let us consider a few aspects of the model. At $\beta = 0$ the model is accurate in the sense that all points in both the model and experiments return to the same cross-sectional locations. For $\beta > 0$ the picture is only qualitatively correct; for example, figure 9 compares the shape of streaklines

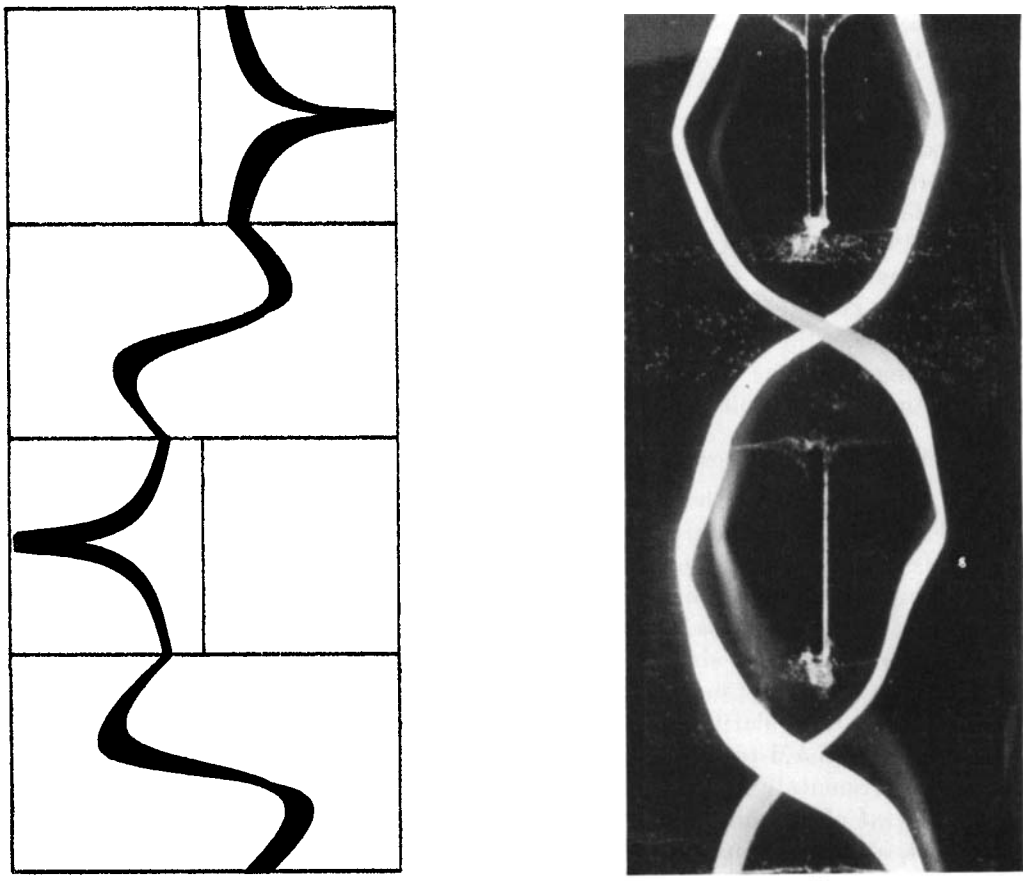

(a) (b)

FIGURE 9. Comparison of streaklines inside period-2 KAM-tubes in the PPM experiments and the model. Two mixer segments are shown. (*a*) Streakline computed from the model at mixing strength $\beta = 8$. (*b*) Streakline from experiment at mixing strength $\beta = 10 \pm 0.3$, $Re_{\text{PPM:axial}} = 0.3$, and $Re_{\text{PPM:cs}} = 1.8$.

inside the period-2 KAM-tubes for a computation at $\beta = 8$ and an experiment at $\beta = 10$. The experiments show two streaklines, each within a KAM-tube. The cross-sectional flow of the model is stronger than observed experimentally so the streakline deforms more in each mixer element. The experimental streakline is smooth while the jumping from one stream surface to another in the model gives rise to non-smooth streaklines. Comparison of numerical and experimental streaklines in KAM-tubes at higher values of β is simply not possible; computations yield no period-2 elliptic points in the Poincaré section for $10 < \beta < 40$. By $\beta = 10$ the model predicts that the period-2 KAM-tubes no longer exist; in fact the period-2 fixed points predicted by the model turn out to be hyperbolic; figure 10 shows PPM model Poincaré sections and period 1–3 periodic points for $\beta = 8$ and 10. In general the PPM model predicts many more bifurcations than were observed in the experiments whereas the experiments indicate that KAM-tubes are stable for β between 10 and 25 (and maybe even 30). The model, however, is very useful in screening variations in mixer designs. For example, an important aspect that influences the mixing is the sense of rotation of adjacent mixer elements; such issues can be investigated in terms of symmetries (Franjione & Ottino 1992).

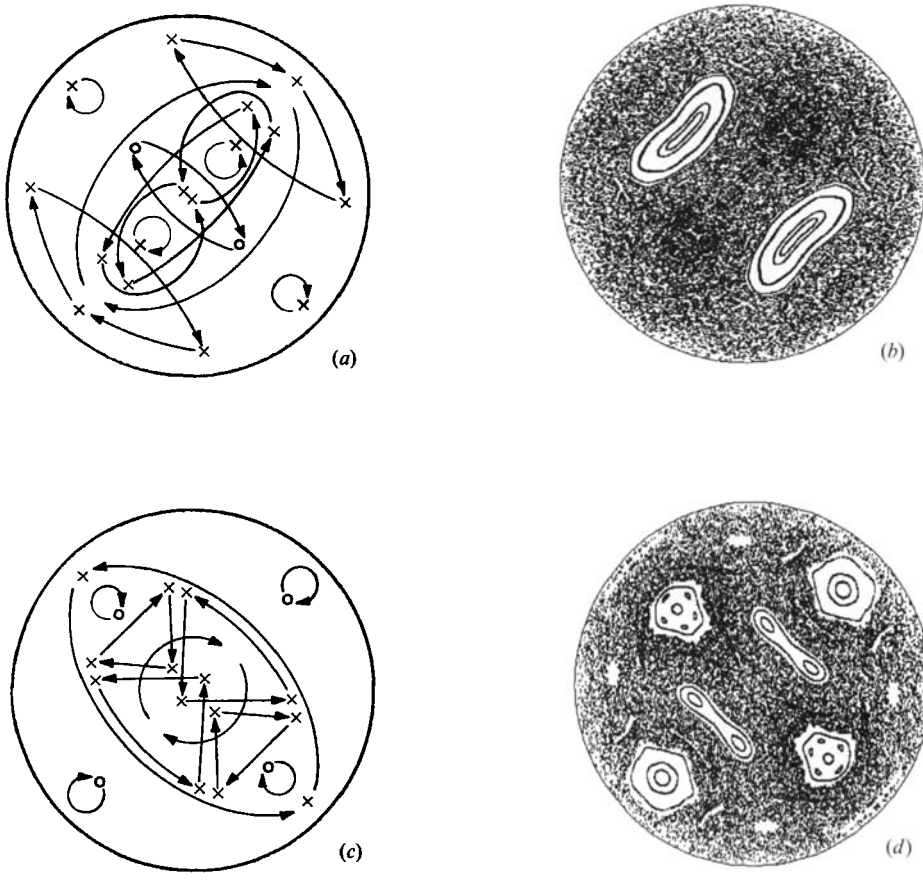

FIGURE 10. Positions and motions of periodic points in the cross-section of the PPM (a, c) and corresponding Poincaré sections (b, d). The crosses represent hyperbolic points and the circles elliptic points; the periodic points are for periods 1–3. The mixing strength is (a, b) $\beta = 8$; and (c, d) $\beta = 10$. Note the island exchange in the case $\beta = 8$.

Chaotic mixing experiments in time-periodic two-dimensional flows quickly reveal a large-scale dye-pattern structure that forms a template for subsequent evolution of stretching and folding; further action of the flow produces stretched and folded striations which are nested within the original template. Moreover, the structure is remarkably independent of the initial position of the dye blob, providing that the blob is placed somewhere in the chaotic region. Large-scale structures in two-dimensional flow experiments return to their initial positions at the end of each period; a similar mechanism operates in spatially periodic flows. It should be pointed out that there are some difficulties in identifying the asymptotic structure in spatially periodic continuous flows; the main difficulty is that it is rather difficult to see the mixed structure internal to the flow. The most visible structures are the ones closest to the outer cylinder and structures internal to the flow are therefore obstructed. Another problem is that the dye concentration is the lowest where the stretching is the most intense and higher where the stretching of the dye is less intense. Therefore we are less likely to see the structures most responsible for generating the good mixing.

We identify three structures in the PPM at a mixing strength of $\beta = 10$ that appear to be periodic; see figures 7(b), 7(c) and 8(c). The first is the streaming flow

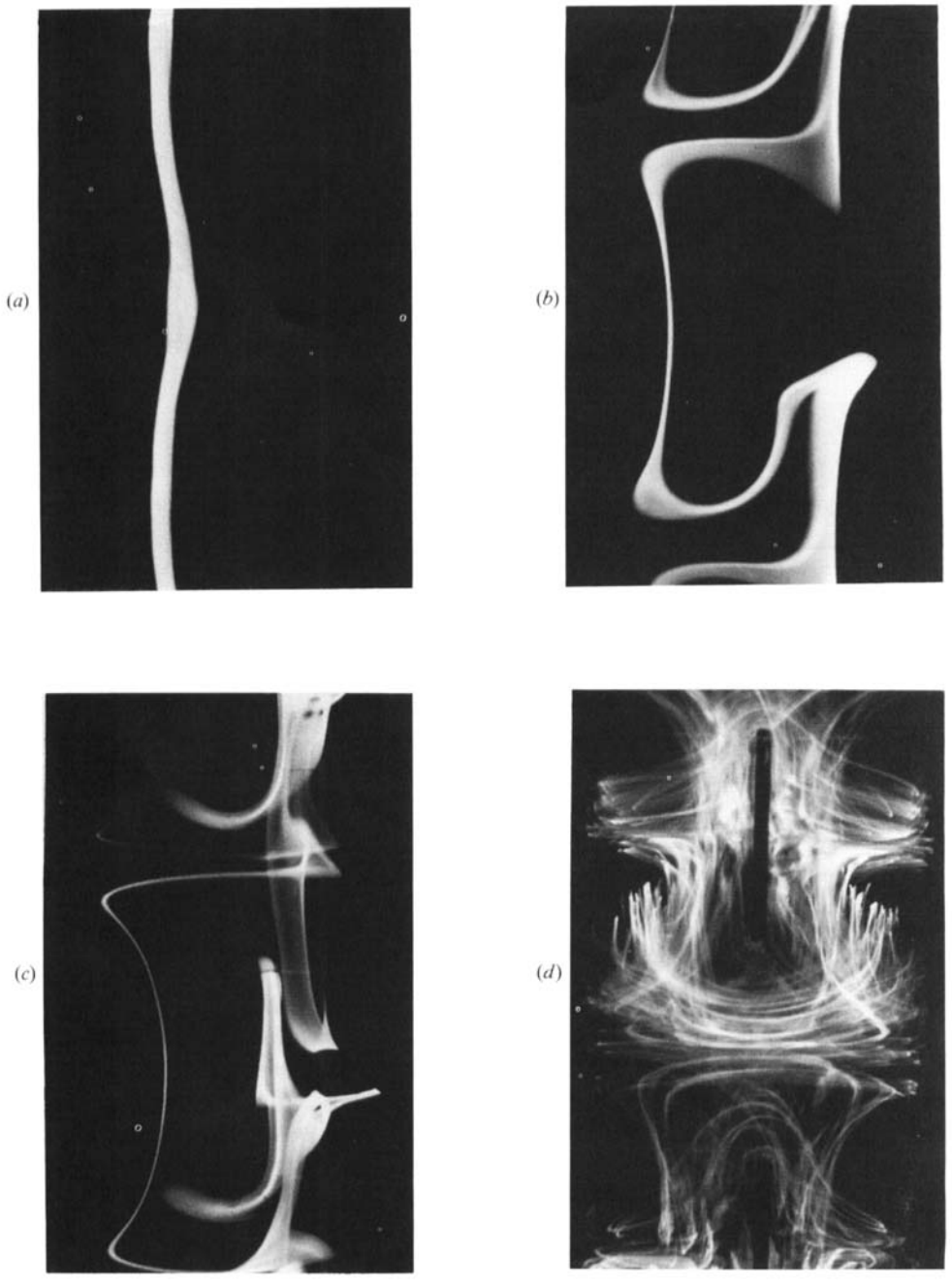

FIGURE 11. Time development of mixed structures in PPM system with no axial flow ($\beta = \infty$). The angular velocity of the cylinder is $v_R = 0.88 \pm 0.01$ cm/s. (*a*) The initial condition of the dye streak, (*b–d*) the dye structure at later times.

past the plates perpendicular to the paper; the second is the cusps near the outer cylinder; and the third is the period-2 KAM-tubes in the flow. As the fluid moves down the mixer, structure is added as additional folds and striations in the chaotic regions. There are, however, small-scale details that are different from experiment to

experiment, and indeed that are not spatially periodic in one experiment. These are attributable to differences in the initial conditions and to slight aperiodicities in the experimental geometry.

4.1.3. *Mixing with no axial flow*

The case $\beta = \infty$ corresponds to mixing with no axial flow and serves to reveal the role of backflows. The initial condition is set as follows: we run the mixer at $\beta = 0$ (no cross-sectional flow) and produce a single dye streak that travels almost straight through the mixer (see figure 8*a*); we then turn off the dye and stop the axial flow. The initial condition is shown in figure 11 (*a*). When the cross-sectional flow is turned on, the dye is deformed as is shown in figure 11 (*b–d*). In figure 11 (*b*) the dye streak has approached the plates perpendicular to the page and parts have continued past. In figure 11 (*c*) the dye has moved above and below the plates in the plane of the page and continued to the back half of the plate perpendicular to the page. After the flow has been run for several minutes the dye has deformed as shown in figure 11 (*d*) (the position of the plates is clear in figure 11*d*, although it is slightly different than the position in figure 11*a–c*). Several symmetries are apparent; the system consists of cells spanning two neighbouring half-plates. This is an experimental example of a bounded, steady three-dimensional chaotic Stokes flow. In this context we cite the exact solutions to the Stokes equations that show chaotic streamlines for a steady flow inside a sphere found by Bajer & Moffat (1990) and Stone *et al.* (1991).

4.1.4. *Effect of Reynolds number*

Implicit in the results presented above is the assumption that the experimental system is completely characterized by β and that results are indeed independent of the Reynolds number. In order to test this assumption several sets of experiments were run keeping the dye injection constant, but varying the Reynolds numbers. Four results are shown in figure 12 corresponding to $\beta = 4$. Only parts of the mixer are shown to highlight small variations. Figures 12 (*a*) and 12 (*b*) show only the fifth to seventh mixer segments whereas figures 12 (*c*) and 12 (*d*) show the second to fourth segments. The streaklines are remarkably similar in spite of significant variation of the Reynolds numbers. Differences are primarily due to small fluctuations in the thickness of the dye streak at the injection point. Similar experiments were carried out at higher values of the mixing strength. It does appear that, within experimental error, inertial effects are unimportant at the operating conditions used in the experiments and that the system is completely characterized by the mixing strength β.

4.2. *An example of a time-periodic system: the EHAM flow*

The eccentric helical annular mixer (EHAM) provides a useful counterpart for comparison of the results obtained in the previous Section. The cross-section of this system corresponds to the flow between eccentric cylinders and the axial flow is a pressure-driven Poiseuille flow. In this case the system is time-periodic rather than spatially periodic and the solution for the velocity field, under Stokes flow, involves no additional approximations. Both regular and chaotic regions are advected by the flow.

4.2.1. *Steady EHAM flows*

The simplest experiments correspond to steady flows. Two typical cases are considered; companion computations are presented as well. When the cylinders turn in the same direction, the cross-sectional streamlines are deformed circles and the

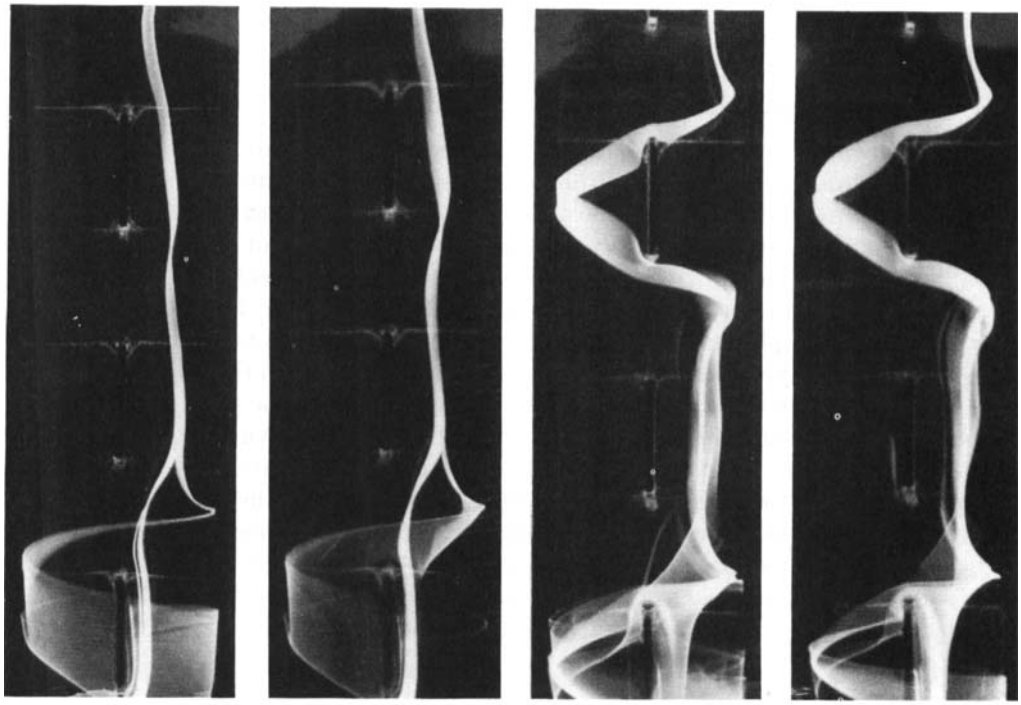

FIGURE 12. A comparison of mixing in the PPM with constant mixing strength but varying Reynolds numbers. The mixing strength parameter $\beta = 4 \pm 0.1$ (a, c) and 4 ± 0.2 (b, d) and Reynolds numbers are: (a) $Re_{\text{PPM:axial}} = 0.6$, and $Re_{\text{PPM:cs}} = 1.3$; (b) $Re_{\text{PPM:axial}} = 0.4$, and $Re_{\text{PPM:cs}} = 0.8$; (c) $Re_{\text{PPM:axial}} = 0.4$, and $Re_{\text{PPM:cs}} = 1.0$; and (d) $Re_{\text{PPM:axial}} = 0.3$, and $Re_{\text{PPM:cs}} = 0.7$.

streaklines are skewed helices; see figures 13(a) and 13(b). When the cylinders turn in opposite directions there are two critical points in the cross-sectional flow (see figure 2b). A dye streak placed near the elliptic point in the cross-sectional flow does not go around the inner cylinder, but stays out in the large-gap region of the flow, spiralling around the elliptic point; see figures 13(c) and 13(d). The agreement between experiments and computations is excellent. Notice that in both cases the dye streaks grow in thickness linearly as they travel down the tube, as predicted in §2.1.

4.2.2. *Time-periodic flows*

The EHAM flow can be made chaotic by operating the cylinders at a time-periodic manner. A possible velocity dependence can be written as

$$v_k = R_k \Omega_k \left[1 + \delta_k f_k \left(\frac{t}{T_k} \right) \right], \quad k = 1, 2, \tag{33}$$

where v_k is the linear velocity of the cylinders, R_k the cylinder radius, Ω_k the mean angular velocity, δ_k the magnitude of the perturbation, T_k the length of the perturbation, f_k the perturbation function, and the subscript $k = 1, 2$ denotes the inner and outer cylinders, respectively. Obviously, a wide range of modulations are possible. For simplicity we restrict ourselves to modulations with unit perturbation

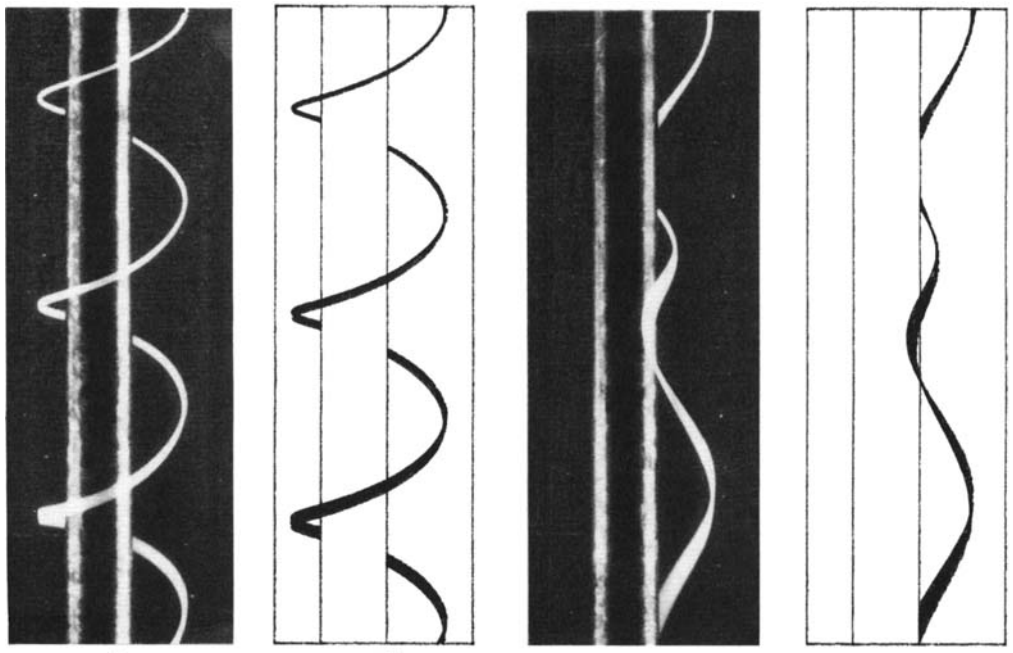

FIGURE 13. Steady experimental (*a*, *c*) and numerical (*b*, *d*) streaklines in the EHAM. The radius ratio and dimensionless eccentricity are 1/3 and 0.3, respectively. The Reynolds numbers and cylinder velocities are (*a*) $Re_{\text{EHAM:axial}} = 0.7$, $Re_{\text{EHAM:cs}} = 6.4$, $v_1 = 1$ cm/s and $v_2 = 1$ cm/s; and (*c*) $Re_{\text{EHAM:axial}} = 0.7$, $Re_{\text{EHAM:cs}} = 6.4$, $v_1 = -1$ cm/s, and $v_2 = 1$ cm/s. The cylinder rotation rates and axial velocities of the numerical streaklines (*b*, *d*) are the same as the experimental streaklines.

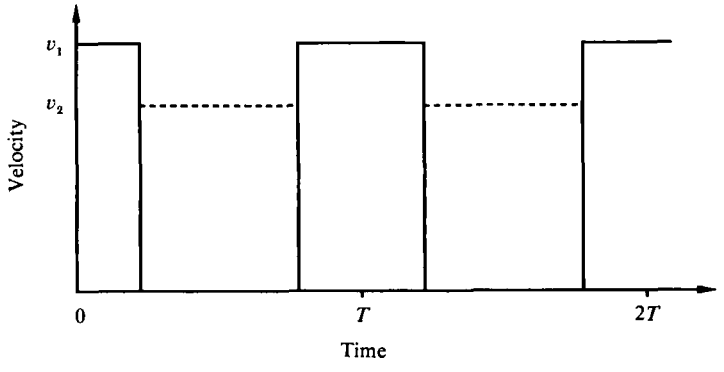

FIGURE 14. Sample square-wave velocity protocol. When one cylinder is turning the other is not. The period of perturbation is defined so that the inner cylinder is turning at the beginning of the period, and so that the protocol is symmetric with respect to the origin of time ($t = 0$). v_1, Inner cylinder velocity; v_2, outer cylinder velocity; T, period of perturbation.

($\delta_k = 1$) and square wave velocities, i.e. only one cylinder is turning at a time (see figure 14). Notice that the origin of time, the starting condition for the experiments, is chosen as halfway through the motion of one of the cylinders. Swanson & Ottino (1990) showed this protocol generates symmetric Poincaré sections and facilitates the investigation of periodic points.

The starting point for analysis of chaotic motion is provided by Poincaré sections

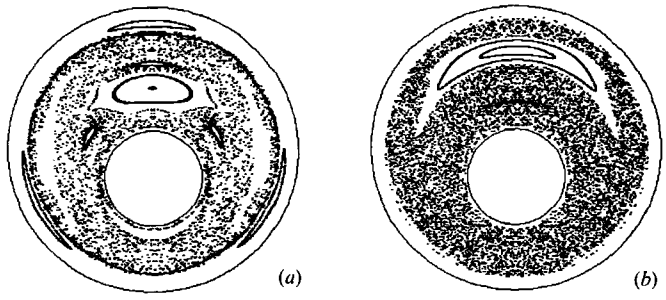

FIGURE 15. Journal-bearing Poincaré sections for the 540° and 1080° cases. The eccentricity and radius ratio are 0.3 and 1/3, respectively. Square-wave velocity protocols are used. The inner cylinder turns (*a*) 540° and (*b*) 1080° per period. The outer cylinder turns half as many degrees per period.

of the two-dimensional flow between eccentric cylinders. Figure 15 shows two typical Poincaré sections; the difference between flows is the angular rotation of the cylinders per period. In figure 15(*a*) the inner cylinder turns 540° per period, and in figure 15(*b*) the inner cylinder turns 1080° per period; the outer cylinders turn half as many degrees as the inner cylinders (subsequently the flows will be referred to by the number of degrees the inner cylinder turns per period). The primary feature of interest is the large period-1 islands (see Swanson & Ottino 1990). Small dye blobs initially placed in the chaotic regions of the two-dimensional flows (identified in the Poincaré sections as the region where trajectories wander randomly) quickly stretch and fold to cover the entire chaotic region while dye blobs placed in islands barely stretch or deform at all. What happens in similar experiments done in the EHAM? Figures 16(*a*) and 16(*b*) (plate 4) show the results obtained by injecting a dye streak into the large regular regions of both flows, and in figure 16(*c*) and 16(*d*) (plate 4) a second dye streak is added in the chaotic regions. There is a large difference between the results. The results of the 540° case are what we expect by extrapolating from two-dimensional chaotic flows results, while the results of the 1080° case are somewhat unexpected. Notice the parts of the green dye streak directly beneath the injection point; those portions of the dye streak are behaving similarly to the 540° case, while the other portions are being well mixed. The dye streak seems to be partially chaotic and partially regular. It is apparent that Poincaré sections of the two-dimensional cross-sectional flow do not contain all the information necessary to predict the gross mixing behaviour of the EHAM flow.

There are two possible reasons for this behaviour. The first is that, as defined, the Poincaré section is independent of the axial flow. At first glance we might try to patch up this deficiency by choosing an axial lengthscale so that the surfaces of section are equally spaced planes. A Poincaré section might then be constructed by recording intersections of a few initial conditions with the surfaces of section. This, however, does not improve the picture: the Poincaré sections so defined are smeared and show little structure since particles arrive at the surfaces at different times during the period of the cross-sectional flow perturbation. The second reason is the manner in which the dye is introduced into the system. Whereas in a two-dimensional flow the dye blob is introduced and the mixing experiment is then started, in a three-dimensional time-periodic flow, such as the EHAM, the dye injection location is fixed and dye is continuously fed throughout the experiment. Thus, the dye is convected away from the dye injection location by the flow and

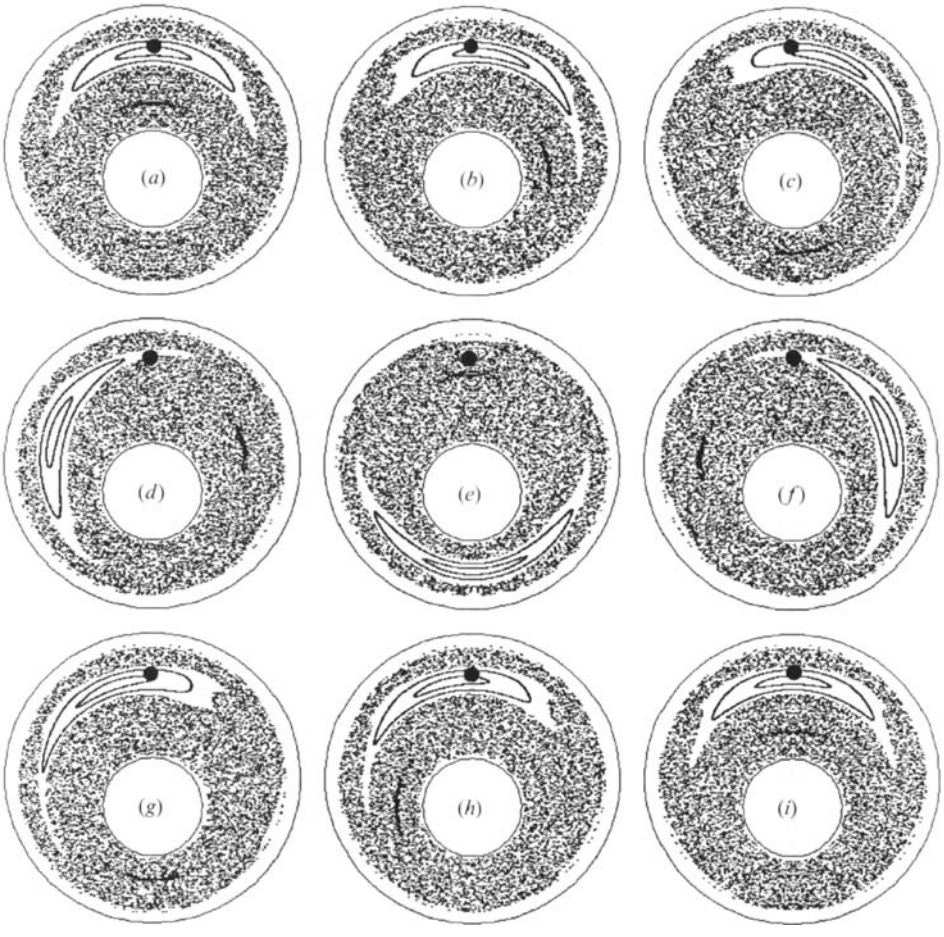

FIGURE 17. Intermediate-time journal-bearing Poincaré sections. The eccentricity and radius ratio are 0.3 and 1/3, respectively. Square wave velocity protocols are used. The inner cylinder turns 1080° per period and the outer cylinder turns 540° per period. The Poincaré sections are taken at (*a*) the beginning of the period; and (*b*) $\frac{1}{8}$; (*c*) $\frac{1}{4}$; (*d*) $\frac{3}{8}$; (*e*) $\frac{1}{2}$; (*f*) $\frac{5}{8}$; (*g*) $\frac{3}{4}$; (*h*) $\frac{7}{8}$ of the period; and (*i*) at the end of the period.

thereafter every piece of the streakline acts as a blob in a two-dimensional chaotic flow experiment that also happens to be moving axially. The major difference, however, is that the dye is injected into different regions of the cross-section at different parts of the period; in particular the dye streak might sample both regular and chaotic regions of the flow at *different* times. 'Intermittency' is therefore possible; since the regular regions (islands) move through space, the streakline can find itself in a regular domain for some time, then be trapped in a chaotic region, then escape and undergo 'relaminarization', and so on.

Let us consider the 'intermittency' issue in more detail. Figure 17 shows Poincaré sections for the 1080° case at 0, $\frac{1}{8}$, $\frac{1}{4}$, $\frac{3}{8}$, $\frac{1}{2}$, $\frac{5}{8}$, $\frac{3}{4}$, and $\frac{7}{8}$ of the period. The large dots represent the approximate injection location of the green dye streak shown in figure 16(*b*). In the 1080° case the island moves all the way around the inner cylinder while in similar computations for the 540° case, the island is found to be essentially stationary. As experimental confirmation, streaklines for the 1080° case are shown in figure 18 at the same parts of the period as figure 17. At $\frac{3}{8}$ of the period the poorly

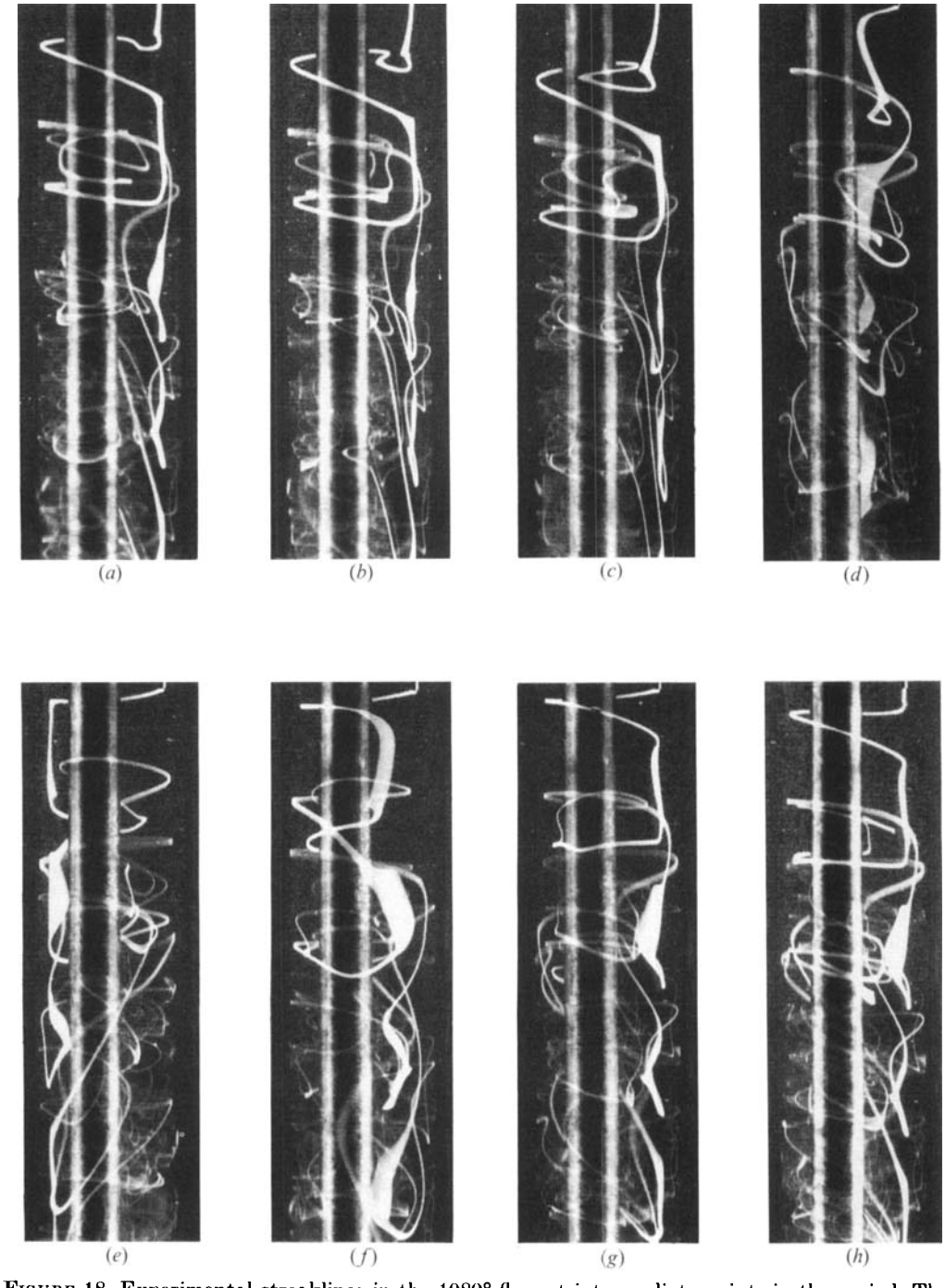

FIGURE 18. Experimental streaklines in the 1080° flow at intermediate points in the period. The radius ratio and dimensionless eccentricity are 1/3 and 0.3, respectively. The Reynolds numbers, and Strouhal number are $Re_{\text{EHAM:axial}} = 0.2$, $Re_{\text{EHAM:cs}} = 4.9$, $Sr = 0.02 \pm 0.0001$. The inner cylinder turns 1080° and the outer cylinder turns 540° per period. The pictures are taken at (*a*) the beginning of the period; and (*b*) $\frac{1}{8}$; (*c*) $\frac{1}{4}$; (*d*) $\frac{3}{8}$; (*e*) $\frac{1}{2}$; (*f*) $\frac{5}{8}$; (*g*) $\frac{3}{4}$; and (*h*) $\frac{7}{8}$ of the period.

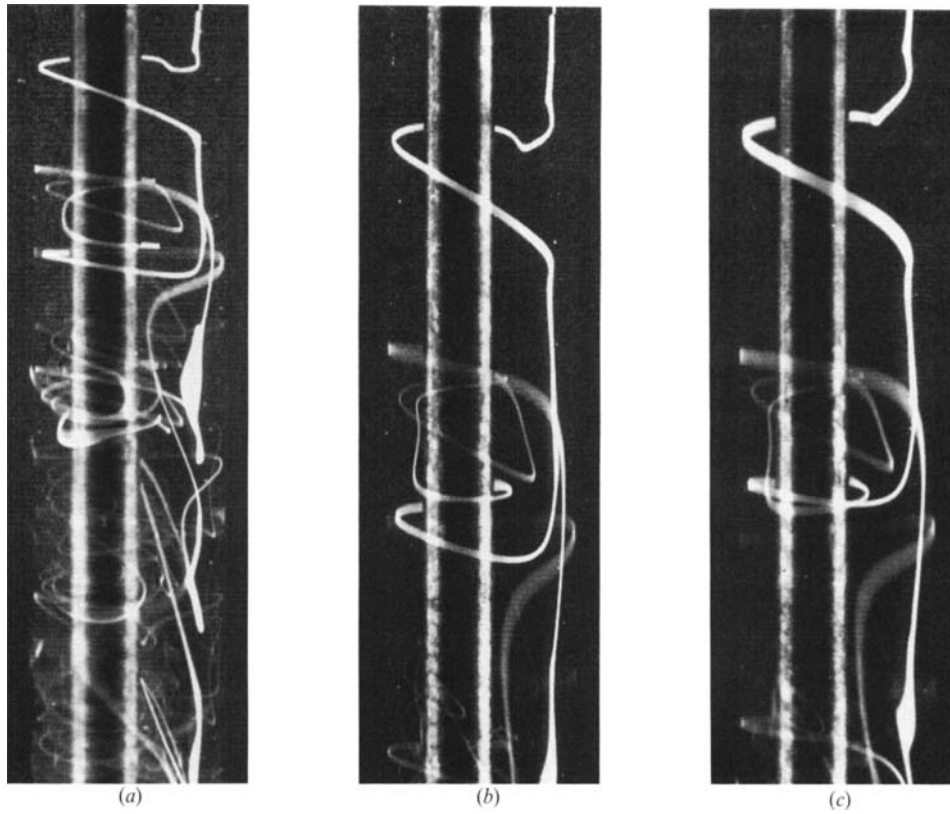

FIGURE 19. Axial flow effect on chaotic EHAM experiments. The radius ratio and dimensionless eccentricity are 1/3 and 0.3, respectively. The inner cylinder turns 1080° and the outer cylinder turns 540° per period. The period of perturbation is 90 s. The Reynolds numbers, Strouhal number and time the inner cylinder turns each period are (*a*) $Re_{\text{EHAM:axial}} = 0.2$, $Re_{\text{EHAM:cs}} = 4.9$, $Sr = 0.02 \pm 0.0001$, $T_{\text{inner}} = 45$ s; (*b*) $Re_{\text{EHAM:axial}} = 0.3$, $Re_{\text{EHAM:cs}} = 4.9$, $Sr = 0.02 \pm 0.0001$, $T_{\text{inner}} = 45$ s; (*c*) $Re_{\text{EHAM:axial}} = 0.3$, $Re_{\text{EHAM:cs}} = 5.2$, $Sr = 0.02 \pm 0.0001$, $T_{\text{inner}} = 30$ s.

mixed dye, or the island, is just moving behind the inner cylinder; at $\frac{1}{2}$ of the period the island is in the small-gap region, opposite its initial position; at $\frac{5}{8}$ of the period the island has just passed in front of the inner cylinder; and at $\frac{7}{8}$ of the period the island has almost returned to its initial position. Islands, or KAM-surfaces, in the two-dimensional chaotic flows give rise to KAM-tubes that move about the cross-section in time when an axial flow is superimposed. It is thus apparent that information from Poincaré sections needs to be supplemented with the dynamics of the motion of KAM-tubes during the period of the perturbation.

4.2.3. *Mixing dependence on the axial flow*

The axial flow does have an impact on the mixed structures created in the EHAM. Such effects are highlighted by the three experiments shown in figure 19. In every case the inner cylinder turns 1080° and the outer cylinder 540° per period. The differences are (i) in figures 19(*a*) and 19(*b*) the inner and outer cylinders each turn for 45 s while in figure 19(*c*) the inner cylinder turns for 30 s and the outer cylinder for 60 s; and (ii) in figure 19(*a*) the average axial velocity is about 0.05 cm/s, while in figures 19(*b*) and 19(*c*) it is about 0.1 cm/s. The Poincaré sections for these three conditions (shown in figure 15*b*) are identical (Swanson & Ottino 1990 showed that

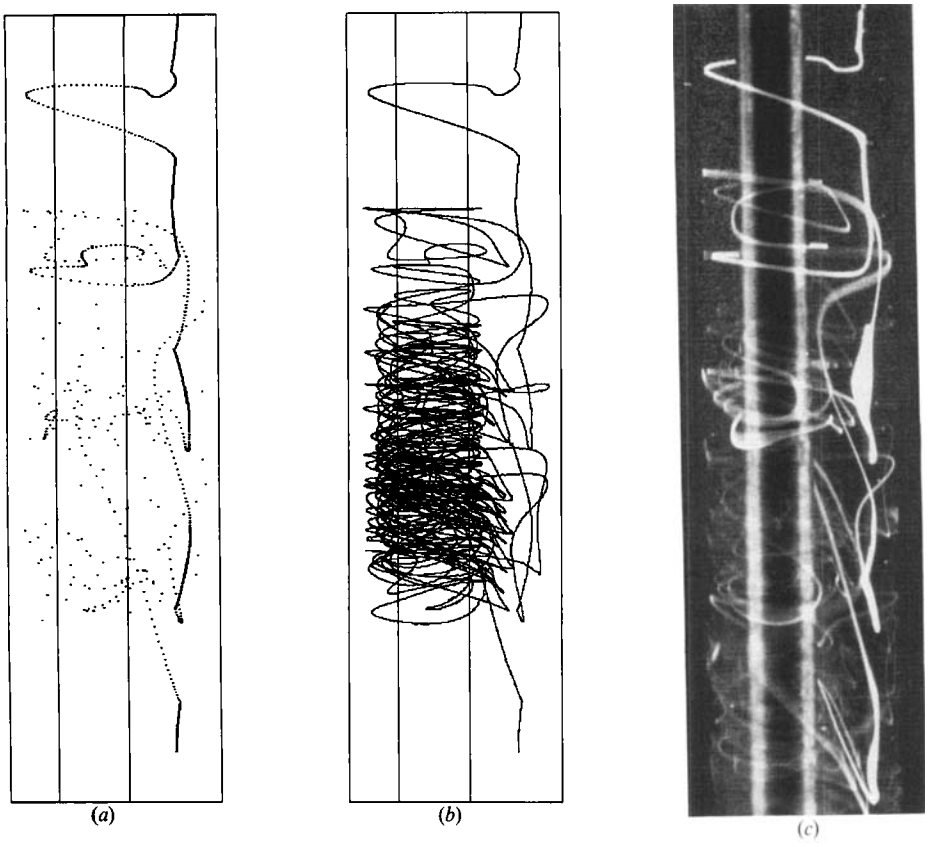

FIGURE 20. Comparison of numerical (*a*, *b*) and experimental (*c*) streaklines in a chaotic EHAM flow. The radius ratio and dimensionless eccentricity are 1/3 and 0.3, respectively. The inner cylinder turns 1080° and the outer cylinder 540° per period. The flow is from top to bottom. The initial positions of the streaklines are in the period-1 island. The numerical streaklines are for 4 periods. The number of points injected is (*a*) constant per period and (*b*) increasing with each period. The Reynolds numbers and Strouhal number for the experimental streakline (*c*) are $Re_{\text{EHAM:axial}} = 0.2$, $Re_{\text{EHAM:cs}} = 4.9$, and $Sr = 0.02 \pm 0.0001$.

the important parameter in the Poincaré sections is the total distance the cylinders turn, not the actual velocity protocols, provided that the flow is in the Stokes regime and that one and only one cylinder is turning at a time). The other similarity in the experimental conditions is that the dye injection location is the same for the three experiments. The dye injection location is chosen so that dye is injected into the KAM-tube for part of the period and into the chaotic region for part of the period.

We start by comparing figures 19(*a*) and 19(*b*). The mixed structures created in the two flows are nearly identical, the primary difference being that figure 19(*b*) has a higher axial flow rate and therefore it moves the mixed dye streak further down the tube. Note, however, that similar parts of the dye streaks have stretched more in the axial direction in the higher flow-rate case. This is probably due to axial dispersion. Figures 19(*b*) and 19(*c*) illustrate a different point: in this case the time each cylinder turns during the period is different, although the sum of the times is the same; the axial flow rates of the two flows are nearly the same. The mixed structures are again very similar; however, there are differences in the shape and relative axial positions of the dye streak. This is due to different cylinder angular velocities; KAM-tubes and

periodic points move at different speeds and therefore explore regions of different axial velocities resulting in different dye structures.

4.2.4. *Numerical streaklines*

Most of the results of the previous sections can be verified numerically. Experiments, however, provide resolution far beyond what is possible computationally. Consider for example the simulation of streaklines. Since the flow is time-periodic, the streakline is changing through the period. The streaklines discussed below are all 'snapshots' of the 1080° case taken at the beginning of a period. The dye injection location is in the KAM-tube. The numerical streaklines are represented by a collection of points. If a constant number of points (300) is injected at equally spaced times through the period, after four periods the streakline has been stretched and deformed, as shown in figure 20(*a*). Parts of the streakline have degenerated into a cloud of points – a manifestation of sensitivity to initial conditions – while the points comprising the part of the streakline in the KAM-tube have barely separated at all. Also, the points in the KAM-tube have moved farther axially than the points in the chaotic region. To fully resolve the streakline, many more points have to be added in the chaotic region. This is where computational limits arise: since points separate exponentially fast in the chaotic region, the number of points required to represent a chaotic streakline grows exponentially in time, leading to the data storage and computational time problems discussed by Franjione & Ottino (1987). The streakline with extra points added, figure 20(*b*) can be compared to the streakline without extra points in figure 20(*a*). Both streaklines are for four periods. This is a reasonable limit for a SUN 4 because this particular streakline required approximately 100 hours of CPU time. An experimental result with an initial position similar to those of the numerical streaklines is also presented in figure 20(*c*) (the experiment is not restricted to four periods). In theory the experimental results could be mimicked numerically by injecting several 'point' streaklines very close to one another. This is impractical, however, and an interpretation based a combination of results such as those in figures 20(*a*, *b*) should be adequate for most practical applications.

5. Conclusions

We have presented the design and operation of a device suited for studies of chaotic mixing in continuous-throughput flows. Two kinds of systems can be readily implemented: steady spatially periodic flows and time-periodic systems; an important special case corresponds to spatially periodic flows with no net axial flow. Representative results were presented in terms of two systems operating in the Stokes regime: the *partitioned pipe mixer*, which is an example of a steady spatially periodic flow, and the *eccentric helical annular mixer*, which is a time-periodic flow. Several other geometries and modes of operation can be easily achieved; two possible configurations amenable to both experimentation and analysis are shown in figure 21. Other modes of operation – beyond that of Stokes flow regime – might include exploiting instabilities such as those leading to Taylor–Couette flow, etc. (Fenstermacher, Swinney & Gollub 1979; Swinney & Gollub 1985). This creates a large array of possibilities for future studies.

The experiments presented here are labour intensive and consume large amounts of fluids. A reduction in the amount of fluids used can be achieved by scaling. A reduction by a factor of one half should be possible; this should allow the use of

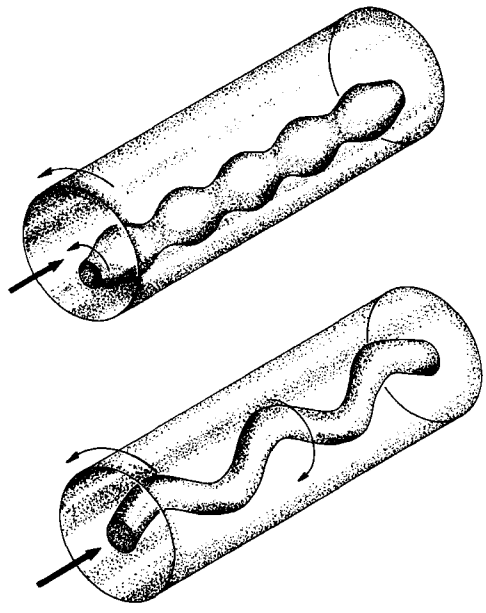

FIGURE 21. Variations on the eccentric helical annular mixer theme.

lower-viscosity fluids without increasing the Reynolds numbers. Larger mixers could also be built; however, more-viscous fluids would be required to maintain Stokes flow conditions. Several problems could profitably be studied in these classes of flows; dispersion and reactive mixing come to mind. However, experimental modifications are necessary. For example, dispersion experiments would require design changes to establish clean injection conditions over the entire cross-section; furthermore, the current set-up is probably not long enough to verify numerical predictions (Jones & Young 1991).

The experimental results obtained in the EHAM flow can be readily substantiated in terms of computations. The model in this instance is exact and the only remaining question is whether computations can be carried out under reasonable time and storage conditions. As pointed out in the past, the resolution provided by experiments can rarely be matched by computations (Ottino *et al.* 1988); an experiment is essentially analogue and computations, no matter how fine grained they are, invariably reveal discretization when initial conditions separate exponentially fast. The agreement between model and computations, however, is more problematic in the case of the PPM. A surprise from the experiments is the robustness of the KAM-tubes; the fact that they exist and are readily observable is gratifying but the fact that they persist under widely different experimental conditions is something that awaits theoretical elucidation. Experiments suggest that the system is dominated by entrance and exit effects and that the flow is fully three-dimensional. Ways of assessing the importance of developing flows are to either carry out a full three-dimensional numerical simulation or to build a series of different mixers with different aspect ratios; neither of these two possibilities seems especially attractive. Another question has to do with stretching within tubes. This is an instance where model predictions are suspect. The simplified model predicts that, under some conditions, the stretching in KAM-tubes can be higher than that in chaotic regions (Khakhar *et al.* 1987); experiments, on the other hand, seem to indicate relatively little stretching within KAM-tubes. Unfortunately there are no realistic spatially

periodic systems to verify these predictions. It should be mentioned that bounded chaotic three-dimensional flow fields, such as those of Stone *et al.* (1991) and Bajer & Moffat (1990), lead to linear stretching within KAM-tubes (see Kusch 1991).

These and other systems might find practical uses, although the goal here was to introduce a flexible device with which one could gain basic knowledge of mixing operations rather than inventing a practical design for specific applications. Applications of chaotic mixing in continuous flow might nevertheless be an incentive for these kinds of studies and it is convenient to record a few observations in this regard. The most obvious use of the apparatus presented here is in the development of basic knowledge for the design of new mixing devices such as those encountered in the polymer industry and biomedical applications; systems can be designed in such a way that a variety of design conditions are satisfied. For example, the mixing can be tailored to increase the speed of mass transfer processes and to accelerate the rate of diffusion-limited chemical reactions. If the fluids are 'delicate' such as bio-fluids, it is possible to design mild-shear-rate histories to avoid breakage and degradation. In many instances mixing requires narrow residence time distributions; this can also be optimized by modifying the forcing in the flow.

It should be stressed as well that some of the results presented here might suggest a rational foundation to time-trusted methodologies arrived at in an empirical or intuitive way; in fact, chaos might be used implicitly in many existing applications. A knowledge of the fundamentals of mixing might allow engineers to look at old processes with new eyes and suggest opportunities for process optimization and invention.

We would like to extend our appreciation to the Fluid Mechanics Division of the National Science Foundation for supporting this work.

REFERENCES

AREF, H. 1984 Stirring by chaotic advection. *J. Fluid Mech.* **143**, 1–21.

AREF, H. 1991 Chaotic advection of fluid particles. *Phil. Trans. R. Soc. Lond.* A **333**, 273–281.

BAJER, K. & MOFFAT, H. K. 1990 On a class of steady confined Stokes flows with chaotic streamlines. *J. Fluid Mech* **212**, 337–363.

CHAIKEN, J., CHEVRAY, R., TABOR, M. & TAN, Q. M. 1986 Experimental study of Lagrangian turbulence in Stokes flow. *Proc. R. Soc. Lond.* A **408**, 165–174.

CHIEN, W.-L., RISING, H. & OTTINO, J. M. 1986 Laminar mixing and chaotic mixing in several cavity flows. *J. Fluid Mech.* **170**, 355–377.

DOMBRE, T., FRISCH, U., GREENE, J. M., HÉNON, M., MEHR, A. & SOWARD, A. M. 1986 Chaotic streamlines in the ABC flows. *J. Fluid Mech.* **167**, 353–391.

FENSTERMACHER, P. R., SWINNEY, H. L. & GOLLUB, J. P. 1979 Dynamical instabilities and the transition to chaotic Taylor vortex flow. *J. Fluid Mech.* **94**, 103–128.

FRANJIONE, J. G. & OTTINO, J. M. 1987 Feasibility of numerical tracking of material lines and surfaces in chaotic flows. *Phys. Fluids* **30**, 3641–3643.

FRANJIONE, J. G. & OTTINO, J. M. 1991 Stretching in duct flows. *Phys. Fluids* A **3**, 2819–2821.

FRANJIONE, J. G. & OTTINO, J. M. 1992 Symmetry concepts for the geometric analysis of mixing flows. *Phil. Trans. R. Soc. Lond.* A (to appear).

HÉNON, M. 1966 Sur la topologie des lignes de courant dans un cas particulier. *C. R. Acad. Sci. Paris* A **262**, 312–314.

JONES, S. W., THOMAS, O. M. & AREF, A. 1989 Chaotic advection by laminar flow in a twisted pipe. *J. Fluid Mech.* **209**, 335–357.

KHAKHAR, D. V. 1986 Fluid mechanics of laminar mixing: dispersion and chaotic flows. Ph.D. thesis, University of Massachusetts, Amherst.

KHAKHAR, D. V., FRANJIONE, J. G. & OTTINO, J. M. 1987 A case study of chaotic mixing in deterministic flows, the partitioned pipe mixer. *Chem. Engng Sci.* **42**, 2909–2926.

KUSCH, H. A. 1991 Experiments on continuous chaotic mixing of viscous liquids. Ph.D. thesis, University of Massachusetts, Amherst.

LEONG, C.-W. & OTTINO, J. M. 1989 Experiments on mixing due to chaotic advection in a cavity. *J. Fluid Mech.* **209**, 463–499.

MIDDLEMAN, S. 1977 *Fundamentals of Polymer Processing*. McGraw-Hill.

NOLL, W. 1962 Motions with constant stretch history. *Arch. Rat. Mech. Anal.* **11**, 97–105.

OTTINO, J. M. 1989 *The Kinematics of Mixing: Stretching, Chaos, and Transport*. Cambridge University Press.

OTTINO, J. M., LEONG, C. W., RISING, H. & SWANSON, P. D. 1988 Morphological structures produced by mixing in chaotic flows. *Nature* **333**, 419–425.

PEARSON, J. R. A. 1981 Wider horizons for fluid mechanics. *J. Fluid Mech.* **106**, 229–244.

SNYDER, W. T. & GOLDSTEIN, G. A. 1965 An analysis of fully developed laminar flow in an eccentric annulus. *AIChE J.* **11**, 462–467.

SOLOMON, T. H. & GOLLUB, J. P. 1988 Chaotic particle transport in time-dependent Rayleigh–Bénard convection. *Phys. Rev.* A **38**, 6280–6286.

STONE, H. A., NADIM, A. & STROGATZ, S. H. 1991 Chaotic streaklines inside drops immersed in steady linear flows. *J. Fluid Mech.* **232**, 629–646.

SWANSON, P. D. & OTTINO, J. M. 1990 A comparative computational and experimental study of chaotic mixing of viscous fluids. *J. Fluid Mech.* **213**, 227–249.

SWINNEY, H. L. & GOLLUB, J. P. 1985 *Hydrodynamic Instabilities and the Transition to Turbulence*. Topics in Applied Physics, vol. 45, 2nd edn. Springer.

WANNIER, G. H. 1950 A contribution to the hydrodynamics of lubrication. *Q. Appl. Maths* **VIII**, 1–32.

YOUNG, W. R. & JONES, S. 1991 Shear dispersion. *Phys. Fluids* A **3**, 1087–1101.